Informed Multi-scale Approach Applied to the British Columbia Fires of Late Summer 2017

Jon M. Reisner[1], Alexander J. Josephson[2], Kyle J. Gorkowski[2], Eunmo Koo[1], Daniel K. Thompson[3], Dave Schroeder[4], and Manvendra K. Dubey[2]

[1]X Computational Physics Division, Los Alamos National Laboratory
[2]Earth and Environmental Sciences Division, Los Alamos National Laboratory
[3]Canadian Forest Service, Natural Resources Canada
[4]Agriculture and Forestry, Government of Alberta

Key Points:

- Formation of PyroCb
- Ejection of pyro-aerosols
- High-fidelity fire-atmosphere coupled simulations

Corresponding author: Alexander Josephson, `alexanderj@lanl.gov`

Abstract

Pyrocumulonimbus clouds have a complex origin depending on fire dynamics and meteorological conditions. When a pyrocumulonimbus (PyroCb) cloud formation develops and is maintained over a period of time, it can inject significant aerosol into the troposphere and lower stratosphere, resulting in longer term (months to years) climate cooling effects. In this work we investigate the British Columbia and northern Washington wildfires on August 12-13, 2017 using a multi-scale simulation framework. We use the output of a physics based wildfire model (FIRETEC) with parameterized energy, particle, and gas emissions to drive the upper atmospheric aerosol mass injection within a regional cloud resolving model (HIGRAD). We demonstrate that vertical motions produced by latent heat release of the condensation of ice and cloud particles within the PyroCbs induce another 5 km of lifting of the simulated aerosol plume. Primary black carbon and organic aerosols alone may not be enough to explain the observed aerosol burden, thus we show that dust and ash particles can enhance lofted aerosol mass. Additionally, we show that semi volatile organic gases emitted by the fires eventually condense, further increasing the aerosol burden. A simulation with all aerosol mechanisms active, driven by the observed fuel load and environmental conditions, reasonably reproduces an aerosol profile inferred from observational data.

1 Introduction

In the late summer of 2017, fires blazed across interior British Columbia (BC17) creating a provincial state of emergency and causing significant loss of habitat and millions of dollars of damage. Although the effects of these fires was undoubtedly felt most strongly by the Province of British Columbia along with surrounding provinces and states, effects of these fires were also felt globally. This global impact was caused in large part by the formation of pyrocumulonimbus (PyroCb) clouds on August 12-13. These PyroCb clouds injected an estimated 0.1-0.3 Tg of particulate matter into the upper troposphere and lower stratosphere (Peterson et al., 2017, 2018) which were then dispersed and eventually deposited across the northern hemisphere (Ansmann et al., 2018; Baars et al., 2019; Zuev et al., 2019; Boone et al., 2020).

While mega-fires of the order of the British Columbia fires are not common place, neither are they rare in the modern day. However, the formation of PyroCb clouds over these mega-fires (Cruz et al., 2012; Rodriguez et al., 2020), which rapidly shift effects of fire from a regional to a global scale, are not as common, with recent occurrences generating a great deal of concern and study. The phenomena of PyroCb clouds have only become an object of intense interest to the scientific community in the last 15 years, because of their seemingly increasing frequency in this era of changing climate (Di Virgilio et al., 2019) and satellite monitoring. A PyroCb cloud forms when the strong plumes formed by large-scale fires coalescence into a directed updraft that can impact possible mid-level regions of moisture leading to subsequent cloud formation and latent heat release. These PyroCb clouds can cause severe thunderstorms (Zhang et al., 2019; Tory et al., 2018; Dowdy et al., 2017), fire-induced whirls sometimes equivalent to tornados (Allen et al., 2020; Lareau et al., 2018; Kablick et al., 2020), and massive injections of fire-emitted gaseous and particulate species into the statosphere on a scale comparable to small volcanic eruptions (Peterson et al., 2018; Christian et al., 2020). These injected species can remain lofted in the stratosphere for extended periods of time and can be transported on a global scale (Gerasimov et al., 2019; Fromm et al., 2019).

In the last two decades, PyroCb events have been increasingly observed and studied throughout western North America with major events observed near Chrisholm, Alberta in 2001 (Fromm, Shettle, et al., 2008; Fromm, Torres, et al., 2008), Yosemite National Park, California in 2013 (Peterson et al., 2015), the Great Slave Lake, Northwest Territories in 2014 (Kablick et al., 2018), and central British Columbia in 2017 (Ansmann et al., 2018; Baars et al., 2019; Peterson et al., 2018) among others. In addition, a large number of PyroCb events

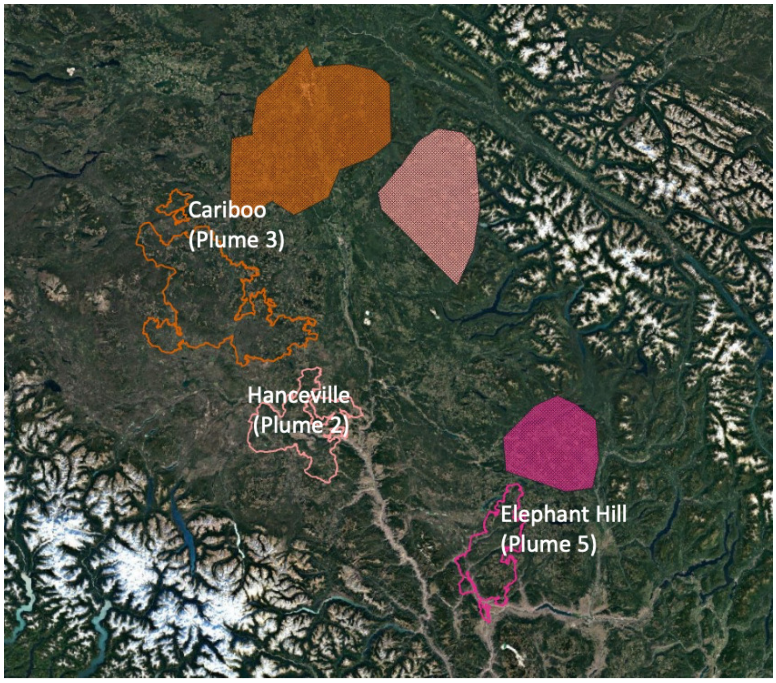

Figure 1. Estimated plume locations (solid polygons) and fire perimeter (outlined polygons) during the time of the PyroCb formation for 3 of the observed PyroCb clouds on August 13, 2017. Fire perimeters estimated using regular overpasses of the VARSII satellite.

have been occurring in recent years around the annual bushfires of southeastern Australia and have garnered significant amounts of interest and study (Fromm et al., 2012; Cruz et al., 2012; Dowdy et al., 2017; Kablick et al., 2020).

Formation of PyroCbs in the BC17 event were enabled by: 1) the availability of atmospheric moisture – i.e. mid-level moisture was moving ahead of an approaching cold front – and 2) deep flaming fires described by Badlan et al. (2021a) (Badlan et al., 2021a, 2021b) which generate intense heat over large areas simultaneously. During the afternoon of the event, a large area of active burning was present, partially the result of numerous slash piles that behave like burning houses, that according to deep flaming theory should support the necessary deep updrafts for PyroCb formation. We will show that particular forest conditions and management practices, in combination with natural factors, led to an increased regional area of active burning which in turn caused the formation of PyroCb clouds at the time of interest.

In this work, we elucidate the BC17 PyroCb cloud formation using an informed multi-scale approach driven by observations. The large spatial scale of the BC17 fire and associated PyroCbs currently prevents use of a detailed combustion model over such a large area. So, to reasonably represent the energy, gas, and particulate formation from regions of active burning, detailed combustion simulations will be undertaken using observed fuels, e.g., a mixture of forest and slash piles from bark beetle kill, over a small area appropriate for that model. The results from these small scale simulations provide forcing terms for a regional-scale model to address PyroCb formation and the transport of aerosols. We will use the regional-scale model results to discuss factors leading to the PyroCb and the resulting aerosol injection profile into the troposphere.

2 Observations

The fires of interest in this study were located in the north-central interior of British Columbia during August 12-13. These fires produced four observed pyrocumulonimbus clouds, and a fifth observed in northern Washington, during the daytime hours with locations captured via satellite. Figure 1 shows an approximate location of three of the five observed plumes, depicted as solid polygons and estimated fire perimeter associated with each of these plumes outlined below each plume. These estimations were made using data from the VARSII satellite overpasses. Note, for this study we neglect the two smallest PyroCbs, formed over northern Washington and further west of the three depicted plumes, due to computational constraints, e.g. simulated aerosol estimates could be underestimated by as much as 20-25 percent given neglect of these two PryCbs.

2.1 Forest Conditions

The northern/central interior of British Columbia has a typical sub-continental climate with cold winters and warm summers. The majority of the rain falls in spring/autumn, and combined with the higher elevations of the interior mountain ranges this region is heavily forested. Of particular interest in this study, is a large area west of Quesnel and north of Alexis Creek British Columbia (approximate coordinates: 52.6 N, -123.4 W). This area is a pine-dominated forest with additional moderate concentrations of Douglas Fir. Using the Canadian National Fuel Inventory and measurements of species in relevant National Fuel Plots (Gillis et al., 2011), a representative forest was recreated with tree characteristics shown in Table 1 and ground fuel characteristics show in Table 2.

In the years leading up to these fires of interest, the interior of British Columbia had experienced an epidemic of Mountain Beetle Kill (Axelson et al., 2009; Perrakis et al., 2014; Dhar et al., 2016). This led to the high mortality rate of Lodgepole Pines and a moderate mortality rate of Douglas Fir as shown in Table 1 and subsequent dead trees were in the 'grey' stage of deterioration, meaning that all foliage had fallen from the tree and accumulated on the ground, but dry branches remained in the canopy. Table 2 shows estimations for ground fuels where the live vegetation represents all non-tree or litter fuels dispersed uniformly across the ground. The litter fuel loads are dispersed directly underneath trees with a maximum fuel load shown in the table and a decay of fuel in proportion to the vertical fuel load of a particular tree species. With the combined forest and ground fuels, total fuel load for the forest were estimated to be 20.53 kg/m^2.

Due to the Mountain Beetle Kill epidemic, large sections of dead forest had been cleared with piles of slash left within the clearings in the years previous to 2017. Satellite imagery from VARSII satellite overpasses prior to the fires showed that many of the slashpiles had yet to be removed prior to the ignited fires and while it is unknown the full extent of slash removal and harvesting activity before the summer fires it is assumed that significant amounts of cured slash fuel remained in the environment at the time of the fires.

2.2 Meterological Conditions

A low pressure system and associated cold front from the west approached the active fire zones over British Columbia on 12 August leading to increased southwest winds both at the surface (8-10 m/s) and aloft (20 m/s at 5 km). Ground temperatures hovered around 27 C and surface relative humidity was less than 40 percent. The stronger winds transported sufficient mid-level moisture over the active fire zones that help support the development of the PyroCbs. For additional details concerning atmospheric conditions on the day of the event see (Peterson et al., 2018).

Table 1. Tree Fuel Characteristics

Tree Species (Common Name)	Pinus Contorta (Lodgepole Pine)	Pseudotsuga Menziesii (Douglas Fir)	Populous Tremulodies (Quaking Aspen)
Fuel Load $\left(\frac{t}{ha}\right)$	174.93	40.92	8.70
Mortality (%)	80	15	0
Tree Height (m)	14.9 (3.7)	19.9 (7.2)	14.6 (4.3)
Height to Canopy (m)	8.6 (2.0)	8.9 (2.9)	9.0 (2.1)
Canopy Diameter (m)	2.5 (1.5)	4.5 (2.0)	3.0 (1.5)
Stems			
Breast Height Diameter (cm)	33.4 (10)	43.3 (10)	22.3 (5)
True Density $\left(\frac{kg}{m^3}\right)$	625	561	689
Moisture Content	50	90	125
Bark Thickness (mm)	7.7	10.0	5.2
Live Canopy Foliage			
Bulk Density $\left(\frac{kg}{m^3}\right)$	1.623	0.578	0.612
Moisture Content	34	10	125
Size-Scale (mm)	0.5	0.5	0.45
Live Canopy Branches			
Bulk Density $\left(\frac{kg}{m^3}\right)$	2.886	1.028	1.087
Moisture Content	50	90	125
Size-Scale (mm)	95 (96)	70 (55)	45 (14)
Dead Canopy Foliage			
Bulk Density $\left(\frac{kg}{m^3}\right)$	0	0	0
Moisture Content	5	5	5
Size-Scale (mm)	0.5	0.5	0.45
Dead Canopy Branches			
Bulk Density $\left(\frac{kg}{m^3}\right)$	2.886	1.028	1.087
Moisture Content	5	8.5	10
Size-Scale (mm)	95 (96)	70 (55)	45 (14)

Tree species macro characteristics in the area of interest. Quantities are average values reported from either the Canadian National Fuel Inventory (Gillis et al., 2011) or measured in National Fuel Plots around the interior British Columbia region. Where available, standard deviation quantities are given in parenthesis.

Table 2. Ground Fuel Characteristics

Ground Fuel Species	Fuel Load $\left(\frac{kg}{m^2}\right)$	Moisture Content	Size-Scale (mm)
Live Vegetation	0.7	6.5	0.5
Pine Litter (Alive)	1.57	0.5	8.5
Pine Litter (Dead)	6.28	0.5	5.0
Fir Litter (Alive)	0.89	0.5	8.5
Fir Litter (Dead)	3.56	0.5	5.0
Aspen Litter	0.50	0.5	10.0

Ground fuels estimations in the area of interest. Live vegetation contains grasses and shrubs, while litter values displayed are peak loads directly underneath trees of the same type.

3 Simulations

Multi-scale simulations were executed to simulate the large range of spatial scales ranging from fires moving though forest and individual slash piles using a combustion model, HIGRAD-FIRETEC, to capturing at a regional scale the formation of PyroCb clouds and injection of particles into the stratosphere using HIGRAD coupled to a cloud model. The high-resolution HIGRAD-FIRETEC combustion simulations of the flame region used reconstructed fuel-maps typical of the environment with results from these simulations being averaged for utilization in the HIGRAD PyroCb regional simulations.

HIGRAD is Los Alamos National Laboratory's (LANL) atmospheric fluid dynamical model that solves either the Euler or Navier-Stokes equation set. For the current effort, the model utilizes a conservative Euler equation set (Ramani et al., 2019) coupled to a cloud physics package (Fierro & Reisner, 2011) that involves the transport and fate of water vapor and various cloud species. Additional transport equations for organic aerosol (OA), black carbon (BC), condensable gases, dust, and ash (DA) have been added along with FIRETEC-derived source terms for these quantities. In addition, secondary organic aerosols (SOA) can be activated with a custom two-product volatility model based on experimentally derived emission factors (Hatch et al., 2017) and a chemical transport model validated volatility distribution (Theodoritsi & Pandis, 2019). The two-product volatility model approach was used for computational efficiency and was tuned to match the OA mass concentration regime in the simulation domain.

FIRETEC is a LANL fire model that when coupled with HIGRAD is designed to resolve with high-fidelity coupled atmosphere-fire behavior and spread on a landscape scale. FIRETEC consists of a variety of physical models to predict atmosphere-fuel interactions (Linn et al., 2012), combustion (Colman & Linn, 2007), heat transfer via convection and radiation (Linn et al., 2005), emission of key particulates like BC and OA (Josephson et al., 2020), the generation and transport of firebrands (Koo et al., 2012), and other fire-generated physical phenomena.

3.1 Localized Fire Simulations

As the area of interest for these fires contained fair amounts of logging in recent years with deposited large slash-piles as detailed in Section 2.1, two simulations were performed to capture the diversity in fuel configurations found in this environment.

The first simulation, or the 'Forest Simulation', was of a virtually-reconstructed untouched forest with roughly the fuel mass concentrations dimensions shown in Table 1 laid out in a domain of 1400 meters by 1400 meters. A 16 meter wide, 1 kilometer long fireline is ignited straddling the center of each domain's y-axis, and 100 meters into the domain along the x-axis; roughly representing a high-intensity fire spreading in from outside the domain. Fuel and fire statistics for this study were computed within the interior 1000 by 1000 meters.

Downwind from the virtually recreated forest, an additional 1400 meters by 1400 meters of resolved domain was added. This extension did not contain any fuel and thus no fire was resolved in these computational cells; rather, these computational cells were added to capture plume evolution beyond the fire domain. In initial simulations, it was found that the fire plume quickly blew out of the original domain and thus we were not able to compute heat flux heights needed for the regional-scale HIGRAD simulations without the addition of the extra cells.

The second simulation, or the 'Slashpile Simulation', contained a rearrangement of fuels in the center square kilometer of fuels into a series of slashpiles. This was done numerically by first removing all the fuels above the first computational cell and reorganizing them into piles that were 20 meters high, 30 meters in diameter, and had a bulk density of roughly 50 kg/m^3 (Hardy, 1998). Before slashpiles were numerically created, 80% of stemwood was removed from the overall fuel distributions as an estimate of the wood removed by the contracted companies as a product (ie., lumber, pulp, etc.) In the square kilometer of treated forest, 16 full slashpiles with the above dimensions and a 17th partial pile were created and evenly distributed throughout the treated area. Ground-fuels, such as grass and forest litter, were untouched with the idea that even though the removal of trees from the area had assuredly altered the ground-fuel landscape, an adequate amount of time had passed to allow ground-fuels to recuperate.

Prior to fire simulations in both domains, a wind "only" simulation was performed where winds were cyclically passed over the entire domain to inform the external boundaries conditions during the actual fire simulation. In each of these wind-runs, the initial wind conditions were informed by the August 13, 2017 Lake Williams Soundings located approximately 115 kilometers south-southeast of the area of interest. With these soundings, initial winds were set to 10 m/s at 30 meters and varied with a 1/7 power-law in the vertical direction (De Chant, 2005).

3.1.1 Results

Due to the high-winds and dry conditions the fire spread rapidly and intensely through this domain, with a fire spread rate of about 80 m/min at its highest peak for the forest simulation and about 110 m/min for the slashpile simulation. During these simulations two distinct regimes of fire activity emerge, the initial flaming regime consisted of high-intensity active burning as the flame front engulfed ground and canopy fuels completely consuming finer fuels and significant fractions of thermally thicker fuels. Figure 2 shows a red isosurface of potential temperature at 350 K for the forest simulation (a) and the slashpile simulation (b), each image is captured 50 seconds after ignition. At this point, the fire front has penetrated deep into the region where statistics are taken and developed it's full shape for both simulations. Due to the mixture of various fuel sizescales and moisture dispersed throughout the domain, the initial fire front for the forest simulation becomes broad and complex as the thicker branches and limbs burn at a slower rate than the finer ground and foliage fuels. On the other hand, the initial fire front in the slashpile simulation is comparatively simple and more narrow as it quickly consumes ground fuel which are much closer to homogenous than the forest canopy fuels. However, as the slashpiles themselves ignite, the overall structure of the fire becomes much more complex as the piles continue to burn long after the fire front as passed. Like the remaining slashpiles, after the fire front

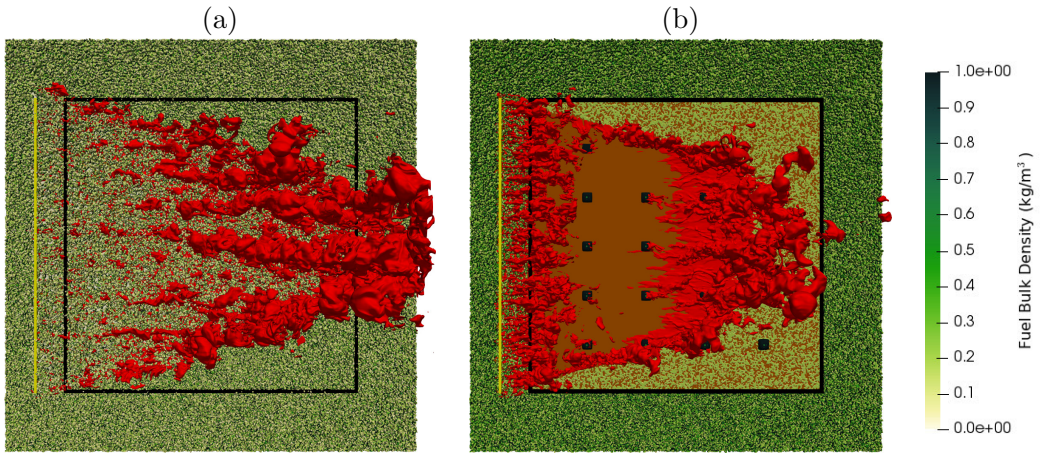

Figure 2. Full flaming regime of the forest simulation (a) and the slashpile simulation (b). Images are captured 50 seconds after ignition and show a red iso-surface of potential temperature at 330 K. The initial fireline is shown in yellow and the areas of interest from which fuel statistics were computed are shown in black.

has passed in the forest simulation these is a significant amount of fuel remaining. This fuel primarily consists of stemwood which is much larger in sizescale then the foliage and branches consumed by the fire front.

Long after the high-intensity fire front has passed, the stemwood of the forest holds enough residual heat to continue to smolder and thus consume further fuel. Figure 3 shows red iso-surfaces of potential temperature at 315 K captured 300 seconds after ignition. For the most part, the smoldering of the Forest, shown in image (a) is very slight with only a few small pockets heated air. In the image, the majority of the iso-surfaces seen along the edges of the domain of interest are due to continued burning of flanking or backing fires outside of the domain of interest but carried by winds into the domain. In contrast, the slashpile simulations produce much more heat in the smoldering regime, with a higher consumption rate of fuel and concentrated plumes originating with each slashpile.

Figure 4 quantifies the total mass consumption rate of fuel within the domain of interest (black boxes of Figures 2-3) as a function of time for both the forest and slashpile simulations. Data from the forest and slashpile simulations are shown in blue and red data points respectively. Image (a) shows the entire FIRETEC simulation, with Image (b) showing a blow-up of the smoldering regime as it is difficult to discern consumption rates on the same scale as the flaming regime. Note that the approximation of the smoldering regime for the forest simulation is notably higher then the simulation results. This increase was used as possible "worst-case" and attempts to take into account the impact of the possible burning tree trunks not accounted for in FIRETEC simulations. The purpose of these FIRETEC simulations is to inform the regional HIGRAD simulation of heat and emission source terms produced by the fires. These source terms are highly dependent on the fire activity and rates of fuel consumption. To approximate the trends seen in the FIRETEC simulation data, we approximated the consumption of fuel as two constant values: one to represent flaming combustion in the first 2000 seconds of simulation time, and a second represent smoldering combustion in times after 2000 seconds.

The approximated constant fuel consumption rates are shown in Table 3. These consumption rates are multiplied by the emission factors, that is grams of a species generated over kilogram of fuel consumed, shown in subsequent rows of Table 3 for the source terms

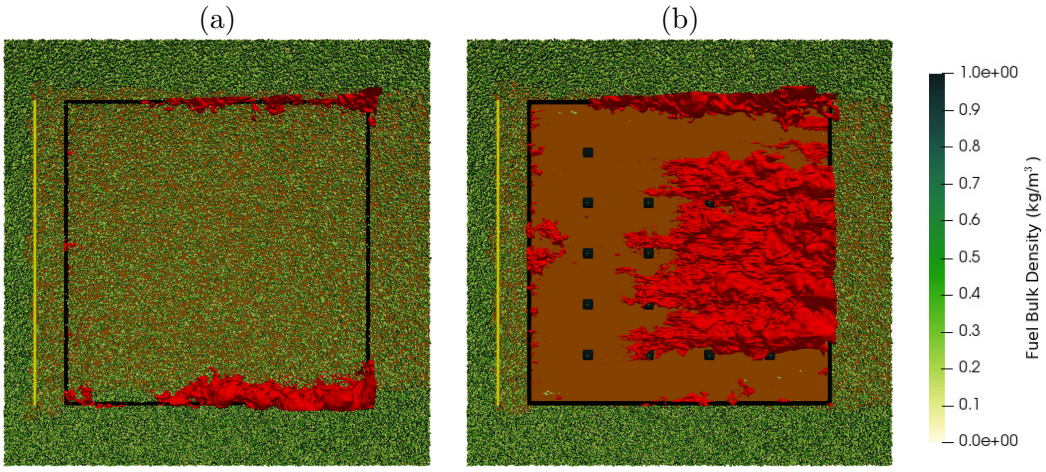

Figure 3. Smoldering regime of the forest simulation (a) and the slashpile simulation (b). Images are captured 300 seconds after ignition and show a red iso-surface of potential temperature at 305 K. The initial fireline is shown in yellow and the areas of interest from which fuel statistics were computed are shown in black.

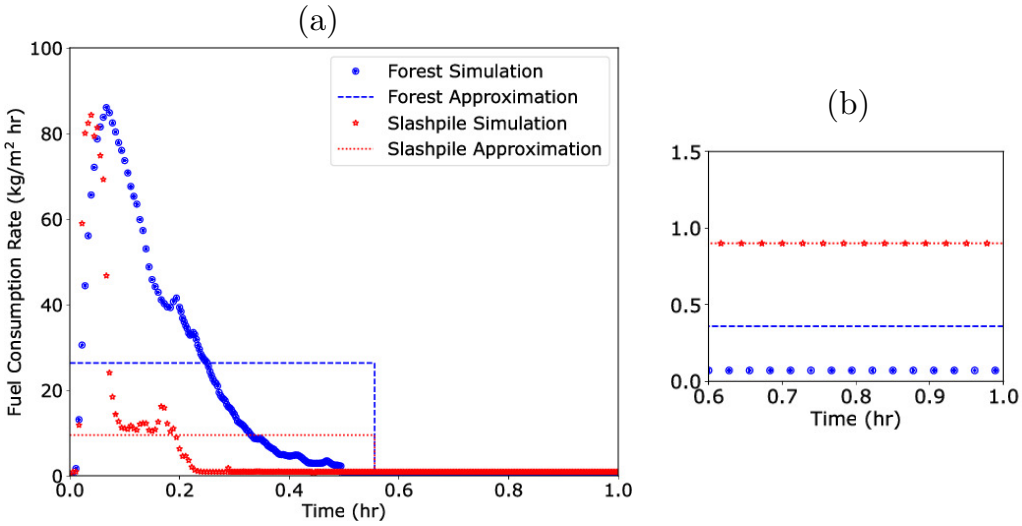

Figure 4. Fuel consumption rates within the forest and slashpile simulations as a function of time. (a) shows the entire duration of the FIRETEC simulations. (b) shows a scale-up of the smoldering regime after the initial 2000 seconds of the simulation.

Table 3. Fire Emission Factors and Fuel Consumption Rates

Gaseous Species	Emission Factor ($\frac{g}{kg}$)
H_2O	775
CO_2	1637
CO	89
O_2	-1212
CH_4	3.92
Other Gases	53.5

Regional HIGRAD Source Term	Forest		Slashpile	
	Flame	Smolder	Flame	Smolder
Fuel Consumption Rate ($\frac{kg}{ha \cdot s}$)	73.21	1	26.37	2.5
PM Emission Factor ($\frac{g}{kg}$)	24	35	30	40
Black Carbon (% of PM)	20%			

Fuel consumption rates fitted from the FIRETEC simulations along with estimated, calculated, and measured emission factors for various major species to be used in the HIGRAD simulation as emission source terms.

of emission generation fed into the regional HIGRAD simulation. The particulate matter (PM) emission factor is calculated directly in the FIRETEC simulations using the zonal-based emission source term model (Josephson et al., 2020). Of these particulate emissions, we estimate 20% to be black carbon (Lee et al., 2022), the rest would be various forms of organic carbon particulates. H_2O emissions come from two sources: 1) the evaporating moisture content of the fuel itself, and 2) a bi-product of the combustion process. We took a weighted sum average moisture content of all the fuels represented in Table 1 for the first part. For the bi-product of the combustion process, we assumed a complete combustion of the elemental composition of Douglas Fir (Biermann, 1996)

$$C_{3.75}H_6O_3 + 3.75\ O_2 \longrightarrow 3.75\ CO_2 + 3\ H_2O. \tag{1}$$

This complete combustion estimation also was used to estimate the negative O_2 emission factor given in Table 3. The other species' emission factors were taken from work done by Akagi et al. (2011) (Akagi et al., 2011) where aerial emission factors for burning temperate forests were measured.

In addition to the mass source terms provided to the regional HIGRAD simulations by the localized FIRETEC simulations, a heat source term was also inferred. At each timestep, an average of potential temperature for all iso-elevated computational cells within the fire plume was taken with results over time are shown in Figure 5. For the purposes of this study, fire plumes were defined as any space where the vertical velocity was greater than 5 m/s, indicating a strong vertical draft. Image (a) of Figure 5 displays the forest simulation and initially created a much stronger vertical plume than the slashpile simulation in Image (b). However, once these simulations entered a 'smoldering phase', at times after 20 minutes, the slashpiles continued to burn at a greater rate than the forest simulations and continued to produce a vertical plume as can be seen the figure. After the initial 'flaming phase', the forest simulation largely ceased to produce a vertical lift.

To integrate these heating results into the regional HIGRAD simulation, an averaged ground plume temperature over each burning regime were taken leading to four distinct heating profiles: 385/340 K for the 'Forest' flaming and smoldering regimes respectively and 380/350 K for the 'Slashpile' flaming and smoldering regimes respectively. Heat was

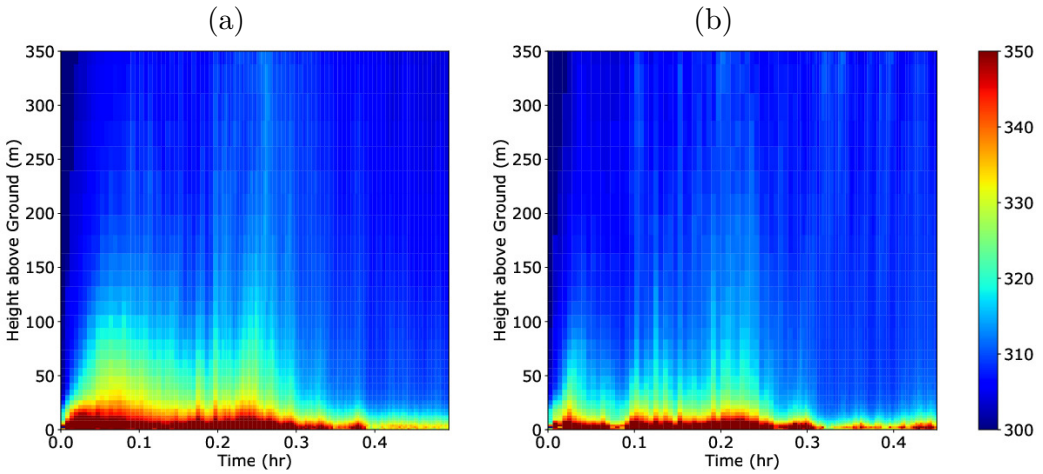

Figure 5. Vertical spatial and temporal evolution of averaged potential temperatures within the fires' developed plumes. Image (a) shows results from the Forest Simulation and Image (b) shows results from the Slashpile Simulation.

added to the regional HIGRAD simulation in proportion to these averaged ground plume temperatures decaying linearly from the ground to 180 meters above the ground where no heat was added at all.

3.2 Regional Atmospheric Simulations

To represent the distribution of fuels in the regional HIGRAD simulation, three different fuel patterns were overlaid on the topography of Interior British Columbia. These three different fuel patterns were: 1) a uniform forest identical to the FIRETEC forest simulation, 2) a series of slashpiles distributed reflective of the FIRETEC slashpile simulations, and 3) a mixed forest/slashpile thought to be more representative of the forest conditions at the time of the fire, this mixed landscape creates a 'checkerboard' of forest and slashpile terrains with each occupying alternating square kilometers. Superimposed on these three different fuel patterns and the topography was an active fire map, shown in Figure 1, estimated by the Canadian Forest Service during the extent of the observed PyroCb formation.

A total of six regional-scale HIGRAD simulations were undertaken to quantify the impact of different fuels (forest, slashpiles, or mixed) and latent heat release with regard to the upward transport of organic aerosol and soot. The simulations were driven by averaged energy and mass sources from FIRETEC with the energy source having a vertical dependence, whereas mass sources for water vapor density, OA density, and BC density were specified in the lowest grid cell or 50 m above the topography. The sources were time dependent with a ramp up phase to induce vertical motions for cloud formation, followed by a relatively short flaming phase in which a majority of energy and mass were released. For three of the six HIGRAD simulations, cloud physics was activated at the end of ramp up phase and will serve as comparison against the three simulations in which the option was not activated. For the current simulations, no attempt was made to model fire spread and its potential impact on PyroCb formation. Note, given the high winds associated with this case, fire spread by spotting of hot embers could be significant with this topic and its associated impact on the PyroCbs being examined in future papers.

The regional-scale HIGRAD simulations were run over a domain of 400 $\times$ 400 km^2 utilizing a stretched horizontal mesh in which an inner square region of roughly 200 $\times$ 200

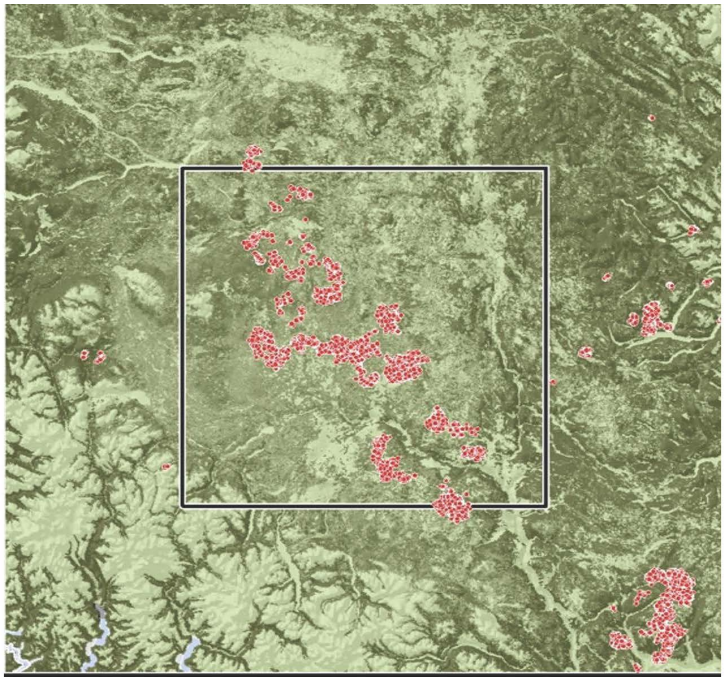

Figure 6. Topography, hot spot data, domain (black box) of 100 m resolution (200 × 200 km^2), and entire domain (400 m resolution outside black box; 400 × 400 km^2) utilized in the HIGRAD simulations.

km^2 was resolved by 100 m spatial resolution and the outer region by 400 m with a total of 2800 × 2800 grid points being employed in the horizontal directions. Vertical resolution was highest near the surface (100 m) and coarser at the model top of 35 km (400 m) with 150 grid points utilized in the vertical. To minimize impact of time-splitting and possible damping of vertical motions, an explicit 2nd order Runge-Kutta solution procedure was employed and used a time step size, 0.05 s, that was limited by the sound speed. Simulations were run on LANL high performance computers with runs typically utilizing between 2500-4900 processors.

Figure 6 shows the topography, the location of the higher-resolution inner grid, and hot spot data supplied by the Canadian Forest service. Within a given simulation, the hot spot data was used as a mask to activate the energy and mass forcing function with the terrain, hot spot data, and forcing functions available upon request. The background horizontal wind, temperature, and gas density fields were initialized using a Spokane Washington sounding taken at 00Z 13 August. Given the relatively short time scale of the simulations, 4 hours, these environmental conditions were assumed constant in time and space. The cloud physics package was similar to the one utilized in (Fierro & Reisner, 2011), except water activation occurred on aerosol injected by the fires, background (750 cm^3), organic, and soot aerosol from the fire, as opposed to just a background aerosol component with all three aerosol assuming $\kappa = 0.1$. Another difference within the cloud physics package was utilization of a ice activation model (Demott et al., 2010) that depends on three quantities, aerosol size, temperature, and ice saturation, as opposed to just two parameters, e.g., Fletcher's curve.

In addition to aerosol produced by the fires, additional sources and transport of condensable gases, dust, ash, and secondary organic aerosol (SOA), were included in two simulations using the mixed fuel type with the only difference being the inclusion of SOA formation in one of the simulations. The dust pickup model utilized was based on threshold velocity (C.

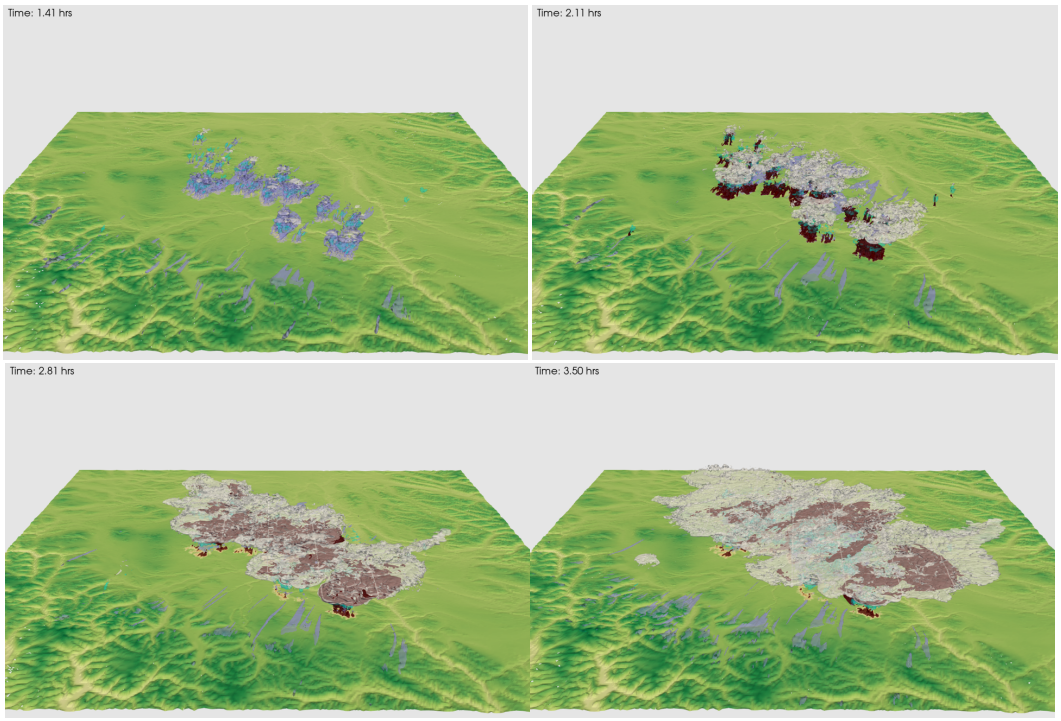

Figure 7. Isosurfaces of various fields, cloud water (turquoise), cloud ice (white), dust/ash (blue), organic aerosol (brown), black carbon (black), and SOA (grey) at 1.5 hrs., 2. hrs., 2.5 hrs., and 3.5 hrs. Terrain is colored by gas temperature with hot spot data, visible at 1.5 hrs., being denoted by red contours.

& Todd, 2012), raised to 10 m/s for the current run, whereas ash production was based on observations that related ash production to fuel type and fire activity (Bahador & Sundén, 2008; Bian et al., 2020) with both fields, ash and dust, being transported in the same computational array. Further, for runs including dust pickup, a land use map was utilized in HIGRAD that turns off the pickup model for land types not supportive of pickup, e.g., undisturbed forest. Likewise, the dust model was limited such that maximum dust densities in a surface cell did not exceed 10^{-5} kg m^{-3} (Ming et al., 2019).

3.2.1 Results

For illustration purposes, Figure 7 shows a time-series of various isosurfaces from a mixed fuel simulation in which all processes were active. As evident in the figures, a rapid upward injection of aerosol occurs during the active fire phase and is in direct response to the specified forcing. Comparison of a mixed fuel simulation against the forest and slash fuel simulations illustrate that this simulation induces more aerosol transport into the upper atmosphere than the slash simulation, but less than the forest simulation. To better quantify this finding, Fig. 8 (top panel) shows the domain integrated time series of total aerosol (OA and BC) from the three simulations (both total and above 10 km) with the forest simulation having the biggest impact in aerosol concentration above 10 km (upper troposphere and lower stratosphere). Overall, results from these three simulations reveal the importance of fuel type on upward injection of aerosol or equivalently the cooler the fire the less upward aerosol transport. Additionally, primary injection of aerosol occurs during the active phase of the fires; however, the mixed simulation does reveal a small ramp up in aerosol production towards the end of the simulation and is associated with the energy

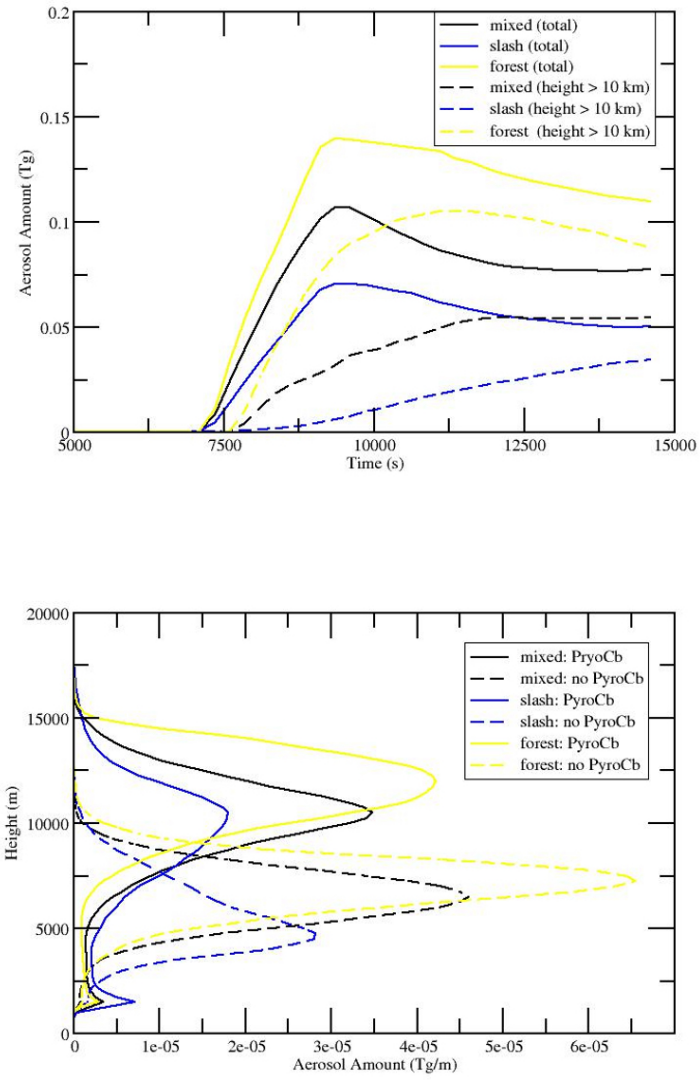

Figure 8. Top panel shows the time history of aerosol, OA and BC, integrated over the entire domain from HIGRAD PyroCb simulations driven by different fuel types, forest, slash, and mixed. Hotter burning fuel, e.g., forest, induces significantly more vertical transport than cooler burning fuel, e.g., slash piles, with a majority of the injection into the upper atmosphere occurring during the active burning phase of the fires. Bottom panel reveals horizontally averaged aerosol amount, OA and BC, from 6 HIGRAD simulations at 3.5 hours with (solid lines) and without (dashed lines) cloud physics active. The impact of latent heat release associated with the simulated PyroCbs is apparent with at least a 4 km rise in the aerosol profiles.

and mass release within the smoldering phases of both the forest and slash piles. Figure 8 (bottom panel) shows horizontally integrated vertical profiles over from all six simulations. The impact of latent heat release is evident with a clear rise in aerosol concentration with this energy release mechanism active. Examination of various energy release processes present in the cloud physics model reveal that the primary energy release was associated with ice condensation or evaporation with future work and data needed to further assess the importance of this process in PyroCb development. For example, for BC17 the tropopause was relatively low, whereas for other events involving higher tropopause heights (Wagman et al., 2020) condensation of water onto the abundant fire produced aerosol may be the primary mechanism for latent heat release.

4 Discussion

4.1 Impact of Other Aerosol Sources

While the three simulations with latent heat active inject significant quantities of aerosol into the upper atmosphere, even for the forest simulation total aerosol amount above 10 km is still on the low end with regard to the observations, e.g., 0.1 versus 0.2 Tg. These low values motivated the need for the two additional simulations that included both dust and ash as well as with the SOA formation active. Indeed, with the addition of dust and ash, aerosol loading does go up throughout the domain with the activation of the SOA formation mechanism another increase in aerosol loading (0.1 Tg) is noted (see Fig. 9). As evident in Fig.9 (top panel), dust pickup is ongoing at 5000 s; however, dust and/or ash is not continually introduced into the upper atmosphere until the time period of significant forcing and formation of the PyroCbs. While dust pickup was evident in the Australian fires (Li et al., 2021) and was suggested in high intensity fires (Wagner et al., 2018), we contend that the simulation represents an upper bound with regard to the amount of dust and ash introduced into the atmosphere for BC17, e.g., unlike Australia no nearby desert is present in British Columbia.

Latent heat associated with the PyroCbs and upward injection of heat from the fires produces a wide area of warmer than ambient temperatures in the upper atmosphere. This temperature excess in combination with continued burning of the slash piles can induce motions that support continued vertical aerosol transport and dust pickup. To examine this, the mixed simulation with dust, ash, and SOA production mechanism active was extended beyond 3.5 hours with Fig. 10 showing that in the lower parts of the atmosphere the production of aerosol still continued and lead to an increase in aerosol above 10 km (0.16 Tg at 3.5 hrs. versus 0.19 Tg at 4 hrs). Beyond 4 hours, significant aerosol mass started exiting the lateral boundaries making inferences regarding whether the aerosol profile will continue to rise difficult; however, the aerosol profile at 4 hours is in the range from what was inferred from observational data (Torres et al., 2020).

4.2 Black Carbon Estimation

Based on climate modeling studies of the BC17 event (D'Angelo et al., 2022), estimated BC mass is 1-2 percent of the total aerosol mass with higher percentages leading to significantly higher rises in the stratosphere than supported by observations. Figure 11 illustrates that for the mixed simulation the BC percentages are considerably higher than supported by observations; however, with the addition of other aerosols BC percentages approach observed amounts. But, additional observational data is needed to quantify the amount of various aerosol present in the upper troposphere and lower stratosphere, e.g., the current simulations may be underestimating OA production and overestimating dust aerosol pickup.

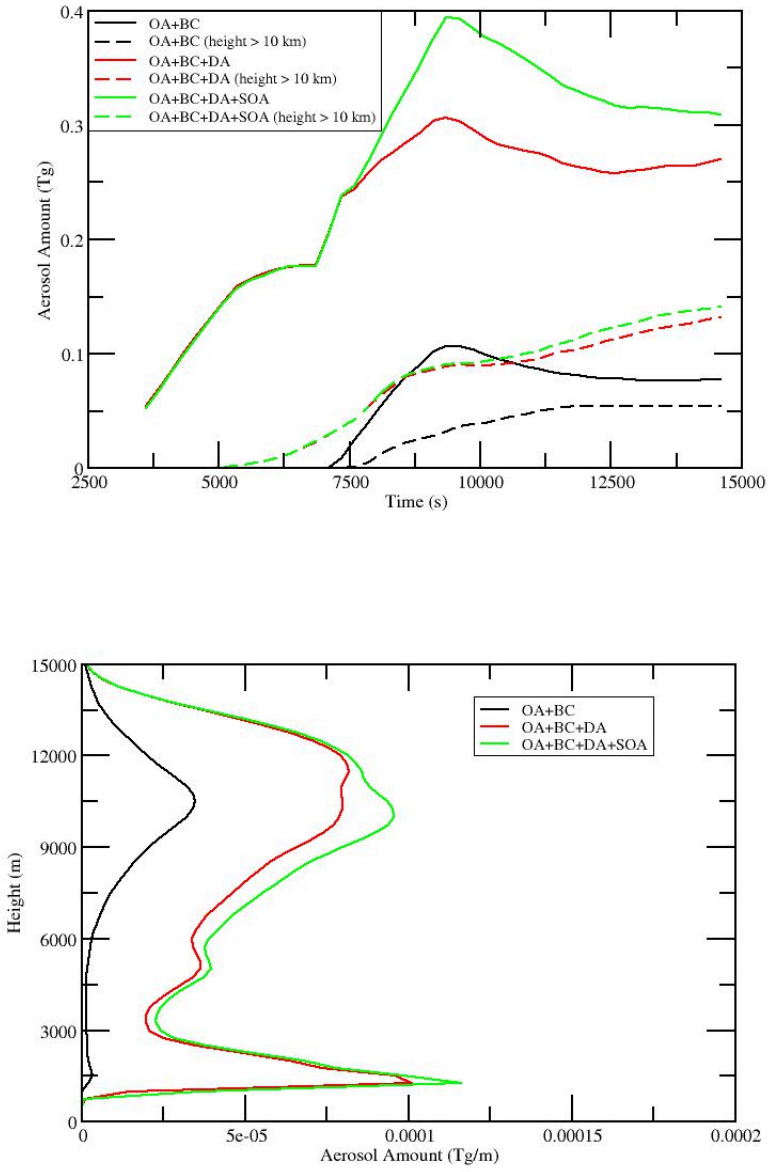

Figure 9. Top panel reveals aerosol amount as a function of time from mixed fuel simulations with BC and OA production active (black lines), BC, OA, and DA production active (red lines), and BC, OA, DA, and SOA production active (green lines). Bottom panel shows horizontally averaged aerosol amount at 3.5 hours from simulations shown in the top panel.

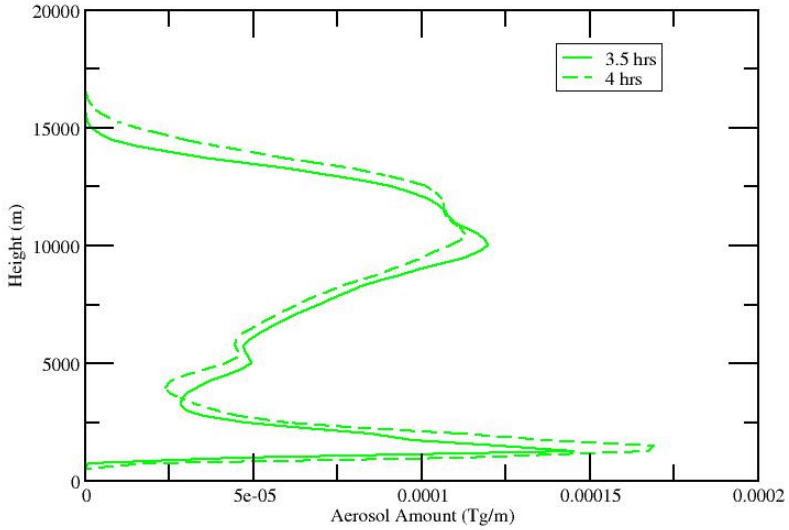

Figure 10. Horizontally averaged aerosol amount from a simulation with all production mechanisms active at 3.5 hours (solid green line) and 4.0 hours (dashed green line).

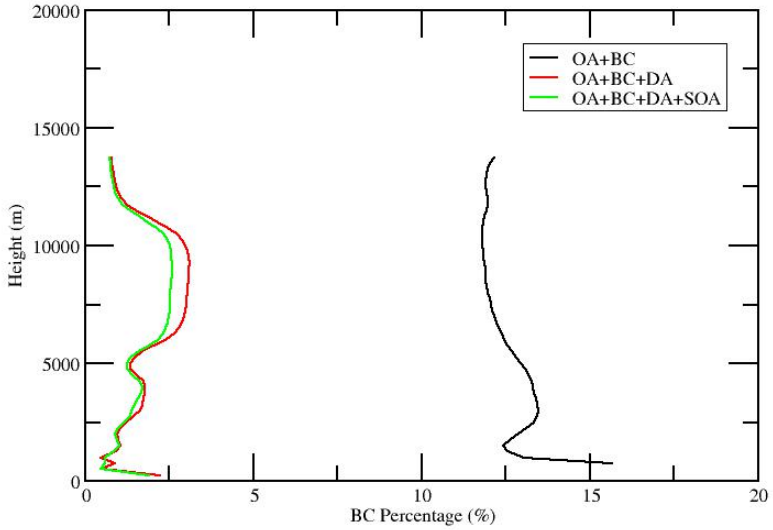

Figure 11. BC percentage as a function of height from the simulation with all aerosol production mechanisms active at 3.5 hours with black line indicating percentage with respect to OA only, red line with respect OA and DA only, and green line with respect to all aerosol.

5 Conclusions

A multi-scale modeling approach was utilized for the BC17 megafire. A novel aspect of this work was the linking of high-resolution combustion simulations to regional scale simulations. The combustion simulations resolve the burning of slash piles and forest with the forest burning significantly hotter than the slash piles. Integral representations of energy and mass release during the active and smoldering phases from the combustion simulations were used in the regional scale simulations and were partially responsible for driving the upward transport of aerosol. And, when latent heat and corresponding PyroCb development is included in the simulations, the aerosol plume rises approximately 5 km over simulations without this mechanism active.

The mixed fuel PyroCb simulation with all aerosol production mechanisms active produced a vertical aerosol profile that roughly agreed with an inferred profile from observations (Torres et al., 2020). But, while this profile could be used to initialize a climate model simulation, it would be of interest to utilize the three dimensional aerosol output to initialize an aerosol plume within a climate simulation using relatively high resolution (25 km or less). Questions regarding the importance of the three dimensional structure of aerosols on potential plume rise within the stratosphere could then be addressed and compared against observed plume dynamics.

6 Open Research

HIGRAD and FIRETEC are export controlled models, but input decks and data can be requested via LANL's Richard P. Feynman Center for Innovation (feynmancenter@lanl.gov).

Acknowledgments

We gratefully acknowledge primary funding for this work provided by a Los Alamos National Laboratory internal lab-directed research and development program. Grant #20200035DR, *Hot Smoke-Dust Signatures to Predict Nuclear Fallout and Winter*. In addition, we gratefully acknowledge the Los Alamos National Laboratory's Institutional Computing Program for providing computational resources for the performed simulations.

References

Akagi, S. K., Yokelson, R. J., Wiedinmyer, C., Alvarado, M. J., Reid, J. S., Karl, T., ... Wennberg, P. O. (2011, may). Emission factors for open and domestic biomass burning for use in atmospheric models. *Atmospheric Chemistry and Physics*, *11*(9), 4039–4072. Retrieved from `www.atmos-chem-phys.net/11/4039/2011/http://www.atmos-chem-phys.net/11/4039/2011/` doi: 10.5194/acp-11-4039-2011

Allen, D. R., Fromm, M. D., Kablick, G. P., & Nedoluha, G. E. (2020, oct). Smoke With Induced Rotation and Lofting (SWIRL) in the Stratosphere. *Journal of the Atmospheric Sciences*, *77*(12), 4297–4316. doi: 10.1175/jas-d-20-0131.1

Ansmann, A., Baars, H., Chudnovsky, A., Mattis, I., Veselovskii, I., Haarig, M., ... Wandinger, U. (2018, aug). Extreme levels of Canadian wildfire smoke in the stratosphere over central Europe on 21-22 August 2017. *Atmospheric Chemistry and Physics*, *18*(16), 11831–11845. doi: 10.5194/acp-18-11831-2018

Axelson, J. N., Alfaro, R. I., & Hawkes, B. C. (2009, apr). Influence of fire and mountain pine beetle on the dynamics of lodgepole pine stands in British Columbia, Canada. *Forest Ecology and Management*, *257*(9), 1874–1882. doi: 10.1016/J.FORECO.2009.01.047

Baars, H., Ansmann, A., Ohneiser, K., Haarig, M., Engelmann, R., Althausen, D., ... Pappalardo, G. (2019, dec). The unprecedented 2017-2018 stratospheric smoke event: Decay phase and aerosol properties observed with the EARLINET. *Atmospheric Chemistry and Physics*, *19*(23), 15183–15198. doi: 10.5194/acp-19-15183-2019

Badlan, R. L., Sharples, J. J., Evans, J. P., & McRae, R. H. D. (2021a, may). Factors influencing the development of violent pyroconvection. Part I: fire size and stability. *International Journal of Wildland Fire*, *30*(7), 484–497. Retrieved from `https://www.publish.csiro.au/wf/WF20040` doi: 10.1071/WF20040

Badlan, R. L., Sharples, J. J., Evans, J. P., & McRae, R. H. D. (2021b, jul). Factors influencing the development of violent pyroconvection. Part II: Fire geometry and intensity. *International Journal of Wildland Fire*, *30*(7), 498–512. doi: 10.1071/wf20041

Bahador, M., & Sundén, B. (2008, may). Investigation on the effects of fly ash particles on the thermal radiation in biomass fired boilers. *International Journal of Heat and Mass Transfer*, *51*(9-10), 2411–2417. doi: 10.1016/J.IJHEATMASSTRANSFER.2007.08.013

Bian, Q., Ford, B., Pierce, J. R., & Kreidenweis, S. M. (2020, jan). A Decadal Climatology of Chemical, Physical, and Optical Properties of Ambient Smoke in the Western and Southeastern United States. *Journal of Geophysical Research: Atmospheres*, *125*(1). Retrieved from `https://agupubs.onlinelibrary.wiley.com/doi/10.1029/2019JD031372` doi: 10.1029/2019JD031372

Biermann, C. J. (1996). *Handbook of Pulping and Papermaking* (2nd ed.). San Diego: Academic Press. doi: 10.1016/B978-012097362-0/50008-X

Boone, C. D., Bernath, P. F., & Fromm, M. D. (2020, aug). Pyrocumulonimbus Stratospheric Plume Injections Measured by the ACE-FTS. *Geophysical Research Letters*, *47*(15). doi: 10.1029/2020GL088442

C., C.-G., & Todd, M. (2012). Modeling simulations of complex dust emissions over the Sahara during the West African monsoon onset. *Advances in Meteorology*, *2012*(25), 1-17. doi: 10.1155/2012/351731

Christian, K., Yorks, J., & Das, S. (2020, oct). Differences in the evolution of pyrocumulonimbus and volcanic stratospheric plumes as observed by cats and caliop space-based lidars. *Atmosphere*, *11*(10). doi: 10.3390/atmos11101035

Colman, J. J., & Linn, R. R. (2007). Separating combustion from pyrolysis in HIGRAD/FIRETEC [Journal Article]. *International Journal of Wildland Fire*, *16*(4), 493–502. Retrieved from `http://www.publish.csiro.au/wf/WF06074` doi: 10.1071/Wf06074

Cruz, M. G., Sullivan, A. L., Gould, J. S., Sims, N. C., Bannister, A. J., Hollis, J. J., & Hurley, R. J. (2012, nov). Anatomy of a catastrophic wildfire: The Black Saturday Kilmore East fire in Victoria, Australia. *Forest Ecology and Management*, *284*, 269–285. doi: 10.1016/j.foreco.2012.02.035

D'Angelo, G., Guimond, S., Reisner, J., Peterson, D., & Dubey, M. (2022). Contrasting stratosphereic smoke mass and lifetime from 2017 Canadian and 2019/2020 Australian megafires: Global simulations and satellite observations. *J. Geophysical Research: Atmospheres*, *127*, e2021JD036249. doi: 10.1029/2021JD036249

De Chant, L. J. (2005, feb). The venerable 1/7th power law turbulent velocity profile: A classical nonlinear boundary value problem solution and its relationship to stochastic processes. *Applied Mathematics and Computation*, *161*(2), 463–474. doi: 10.1016/j.amc.2003.12.109

Demott, P., Prenni, A., X.Liu, Kreidenweis, M., Petters, M., Twohy, C., ... Rogers, D. (2010). Predicting global atmospheric ice nuclei distributions and their impacts on climate. *PNAS*, *107*(25), 11217-11222.

Dhar, A., Parrott, L., Hawkins, C. D. B., Holopainen, J. K., & Martin, T. A. (2016, aug). Aftermath of Mountain Pine Beetle Outbreak in British Columbia: Stand Dynamics, Management Response and Ecosystem Resilience. *Forests 2016, Vol. 7, Page 171*, *7*(8), 171. Retrieved from `https://www.mdpi.com/1999-4907/7/8/171/htmhttps://www.mdpi.com/1999-4907/7/8/171` doi: 10.3390/F7080171

Di Virgilio, G., Evans, J. P., Blake, S. A., Armstrong, M., Dowdy, A. J., Sharples, J. J., & McRae, R. H. D. (2019). Climate Change Increases the Potential for Extreme Wildfires. *Geophysical Research Letters*, *46*(14), 8517–8526. doi: 10.1029/2019GL083699

Dowdy, A. J., Fromm, M. D., & McCarthy, N. (2017). Pyrocumulonimbus lightning and fire ignition on Black saturday in southeast Australia. *Journal of Geophysical Research*, *122*(14), 7342–7354. doi: 10.1002/2017JD026577

Fierro, A., & Reisner, J. (2011). High-resolution simulation of the electrification and lightning of Hurricane Rita during the period of rapid intensification. *J. Atmos. Sci.*, *68*, 477-494.

Fromm, M. D., McRae, R. H. D., Sharples, J. J., & Kablick, G. P. (2012). Pyrocumulonimbus pair in Wollemi and Blue Mountains National Parks, 22 November 2006. *Australian Meteorological and Oceanographic Journal*, *62*(3), 117–126. doi: 10.22499/2.6203.001

Fromm, M. D., Peterson, D. A., & Di Girolamo, L. (2019, dec). The Primary Convective Pathway for Observed Wildfire Emissions in the Upper Troposphere and Lower Stratosphere: A Targeted Reinterpretation. *Journal of Geophysical Research: Atmospheres*, *124*(23), 13254–13272. doi: 10.1029/2019JD031006

Fromm, M. D., Shettle, E. P., Fricke, K. H., Ritter, C., Trickl, T., Giehl, H., ... Deshler, T. (2008, apr). Stratospheric impact of the Chisholm pyrocumulonimbus eruption: 2. Vertical profile perspective. *Journal of Geophysical Research Atmospheres*, *113*(D8), 8203.

Fromm, M. D., Torres, O., Diner, D., Lindsey, D., Vant Hull, B., Servranckx, R., ... Li, Z. (2008, apr). Stratospheric impact of the Chisholm pyrocumulonimbus eruption: 1. Earth-viewing satellite perspective. *Journal of Geophysical Research Atmospheres*, *113*(8). doi: 10.1029/2007JD009153

Gerasimov, V. V., Zuev, V. V., & Savelieva, E. S. (2019, may). Traces of Canadian Pyrocumulonimbus Clouds in the Stratosphere over Tomsk in June-July, 1991. *Atmospheric and Oceanic Optics*, *32*(3), 316–323. doi: 10.1134/S1024856019030096

Gillis, M. D., Omule, A. Y., & Brierley, T. (2011). Monitoring Canada's forests: The National Forest Inventory. *https://doi.org/10.5558/tfc81214-2*, *81*(2), 214–221. Retrieved from `https://pubs.cif-ifc.org/doi/abs/10.5558/tfc81214-2` doi: 10.5558/TFC81214-2

Hardy, C. C. (1998). *Guidelines for estimating volume, biomass, and smoke production for piled slash.* (Vol. 364; Tech. Rep.). Portland, Oregon: United States' Department of Agriculture, Forest Service, Pacific Northwest Research Station. Retrieved from `https://www.fs.usda.gov/treesearch/pubs/26244` doi: 10.2737/PNW-GTR-364

Hatch, L. E., Yokelson, R. J., Stockwell, C. E., Veres, P. R., Simpson, I. J., Blake, D. R., ... Barsanti, K. C. (2017, jan). Multi-instrument comparison and compilation of non-methane organic gas emissions from biomass burning and implications for smoke-derived secondary organic aerosol precursors. *Atmospheric Chemistry and Physics*, *17*(2), 1471–1489. Retrieved from `https://www.atmos-chem-phys.net/17/1471/2017/` doi: 10.5194/acp-17-1471-2017

Josephson, A. J., Castaño, D., Koo, E., & Linn, R. R. (2020). Zonal-Based Emission Source Term Model for Predicting Particulate Emission Factors in Wildfire Simulations. *Fire Technology*. doi: 10.1007/s10694-020-01024-7

Kablick, G. P., Allen, D. R., Fromm, M. D., & Nedoluha, G. E. (2020, jul). Australian PyroCb Smoke Generates Synoptic-Scale Stratospheric Anticyclones. *Geophysical Research Letters*, *47*(13). doi: 10.1029/2020GL088101

Kablick, G. P., Fromm, M. D., Miller, S., Partain, P., Peterson, D. A., Lee, S. S., ... Li, Z. (2018, nov). The Great Slave Lake PyroCb of 5 August 2014: Observations, Simulations, Comparisons With Regular Convection, and Impact on UTLS Water Vapor. *Journal of Geophysical Research: Atmospheres*, *123*(21), 12,332–12,352. doi: 10.1029/2018JD028965

Koo, E., Linn, R. R., Pagni, P. J., & Edminster, C. B. (2012, mar). Modelling firebrand transport in wildfires using HIGRAD/FIRETEC. *International Journal of Wildland Fire*, *21*(4), 396–417. Retrieved from `https://www.publish.csiro.au/wf/WF09146` doi: 10.1071/WF09146

Lareau, N. P., Nauslar, N. J., & Abatzoglou, J. T. (2018, dec). The Carr Fire Vortex: A Case of Pyrotornadogenesis? *Geophysical Research Letters*, *45*(23), 13,107–13,115.

doi: 10.1029/2018GL080667

Lee, J. E., Gorkowski, K., Meyer, A., Benedict, K., Aiken, A. C., & Dubey, M. K. (2022). Wildfire smoke demonstrates significant and predictable black carbon light absorption enhancements. *Geophysical Research Letters*, *In-Review*.

Li, M., Shen, F., & Sun, X. (2021). 2019-2020 Australian bushfire air particulate pollution and impact on the South Pacific Ocean. *Scientific Reports*, *11:12288*. doi: 10.1038/s41598-021-91547-y

Linn, R. R., Anderson, K., Winterkamp, J. L., Brooks, A., Wotton, M., Dupuy, J.-L., ... Edminster, C. (2012, may). Incorporating field wind data into FIRETEC simulations of the International Crown Fire Modeling Experiment (ICFME): preliminary lessons learned. *Canadian Journal of Forest Research*, *42*(5), 879–898. Retrieved from `http://www.nrcresearchpress.com/doi/10.1139/x2012-038` doi: 10.1139/x2012-038

Linn, R. R., Winterkamp, J. L., Colman, J. J., Edminster, C., & Bailey, J. D. (2005). Modeling interactions between fire and atmosphere in discrete element fuel beds [Journal Article]. *International Journal of Wildland Fire*, *14*(1), 37–48. doi: 10.1071/WF04043

Ming, H., Wei, M., & Wang, M. (2019). Quantitative detection of dust storms with the millimeter wave radar in the Taklimakan Desert. *Atmospheres*, *511*(10). doi: 10.3390/atmos10090511

Perrakis, D. D., Lanoville, R. A., Taylor, S. W., & Hicks, D. (2014, aug). Modeling wildfire spread in mountain pine beetle-affected forest stands, British Columbia, Canada. *Fire Ecology*, *10*(2), 10–35. Retrieved from `https://fireecology.springeropen.com/articles/10.4996/fireecology.1002010` doi: 10.4996/FIREECOLOGY.1002010/FIGURES/4

Peterson, D. A., Campbell, J. R., Hyer, E. J., Fromm, M. D., Kablick, G. P., Cossuth, J. H., & DeLand, M. T. (2018, dec). Wildfire-driven thunderstorms cause a volcano-like stratospheric injection of smoke. *npj Climate and Atmospheric Science*, *1*(1). doi: 10.1038/s41612-018-0039-3

Peterson, D. A., Fromm, M. D., Solbrig, J. E., Hyer, E. J., Surratt, M. L., & Campbell, J. R. (2017). Detection and inventory of intense pyroconvection in western North America using GOES-15 daytime infrared data. *Journal of Applied Meteorology and Climatology*, *56*(2), 471–493. doi: 10.1175/JAMC-D-16-0226.1

Peterson, D. A., Hyer, E. J., Campbell, J. R., Fromm, M. D., Hair, J. W., Butler, C. F., & Fenn, M. A. (2015, feb). The 2013 Rim Fire: Implications for predicting extreme fire spread, pyroconvection, smoke emissions. *Bulletin of the American Meteorological Society*, *96*(2), 229–247. doi: 10.1175/BAMS-D-14-00060.1

Ramani, R., Reisner, J., & Shkoller, S. (2019). A space-time smooth artificial viscosity method with wavelet noise indicator and shock collision scheme, Part 2: The 2-D case. *J. Comput. Phys.*, *387*, 45-80. doi: 10.1016/j.jcp.2019.02.048

Rodriguez, B., Lareau, N. P., Kingsmill, D. E., & Clements, C. B. (2020, sep). Extreme Pyroconvective Updrafts During a Megafire. *Geophysical Research Letters*, *47*(18). doi: 10.1029/2020GL089001

Theodoritsi, G. N., & Pandis, S. N. (2019). Simulation of the chemical evolution of biomass burning organic aerosol. *Atmospheric Chemistry and Physics*, *19*(8), 5403–5415. doi: 10.5194/acp-19-5403-2019

Torres, O., Bhartia, P., Taha, G., Jethva, H., Das, S., Colarco, P., ... Ahn, C. (2020). Stratospheric injection of massive smoke plume from Canadian boreal fires in 2017 as seen by DSCOVR-EPIC, CALIOP, and OMPS-LP observations. *J. Geophysical Research: Atmospheres*, *125*(125). doi: 10.1029/2020JD032579

Tory, K. J., Thurston, W., & Kepert, J. D. (2018, aug). Thermodynamics of pyrocumulus: A conceptual study. *Monthly Weather Review*, *146*(8), 2579–2598. doi: 10.1175/MWR-D-17-0377.1

Wagman, B., Lundquist, K., Tang, Q., Glascoe, L., & Bader, D. (2020). Examining the climate effects of a regional nuclear weapons exchange using a multiscale atmospheric modeling approach. *J. Geophysical Research: Atmospheres*, *125*(e2020JD033056). doi:

598 10.1029/2020JD033056
599 Wagner, R., Jahn, M., & Schepanski, K. (2018). Wildfires as a source of airborne mineral
600 dust-revisiting a conceptual model using large-eddy simulation (LES). *Atmos. Chem.*
601 *Phys.*, *18*, 11863-11884. doi: 10.5194/acp-18-11863-2018
602 Zhang, Y., Fan, J., Logan, T., Li, Z., & Homeyer, C. R. (2019, aug). Wildfire Impact on
603 Environmental Thermodynamics and Severe Convective Storms. *Geophysical Research*
604 *Letters*, *46*(16), 10082–10093. doi: 10.1029/2019GL084534
605 Zuev, V. V., Gerasimov, V. V., Nevzorov, A. V., & Savelieva, E. S. (2019, mar). Lidar
606 observations of pyrocumulonimbus smoke plumes in the UTLS over Tomsk (Western
607 Siberia, Russia) from 2000 to 2017. *Atmospheric Chemistry and Physics*, *19*(5), 3341–
608 3356. doi: 10.5194/acp-19-3341-2019

Figure 1.

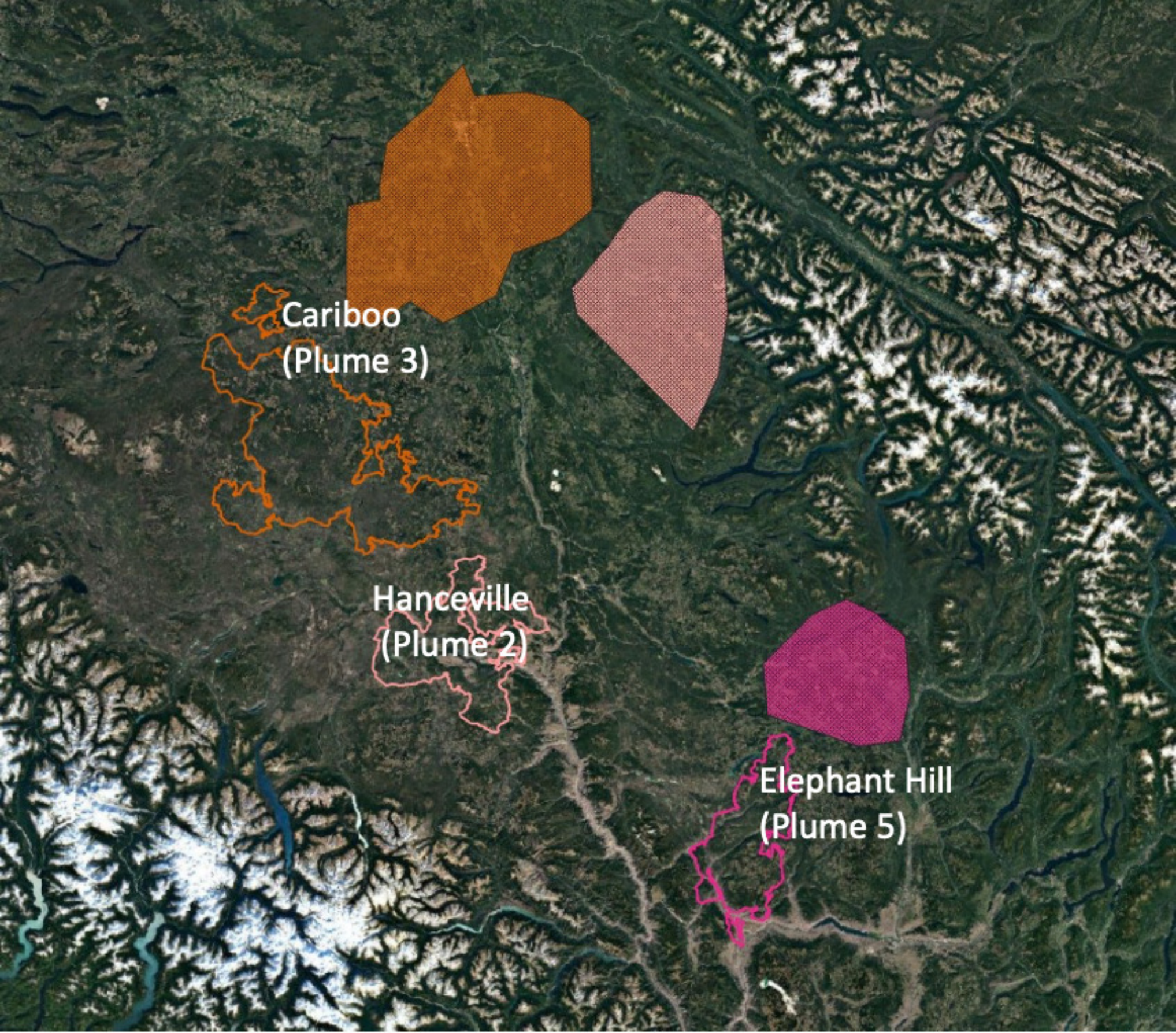
Cariboo
(Plume 3)
Hanceville
(Plume 2)
Elephant Hill
(Plume 5)

Figure 2.

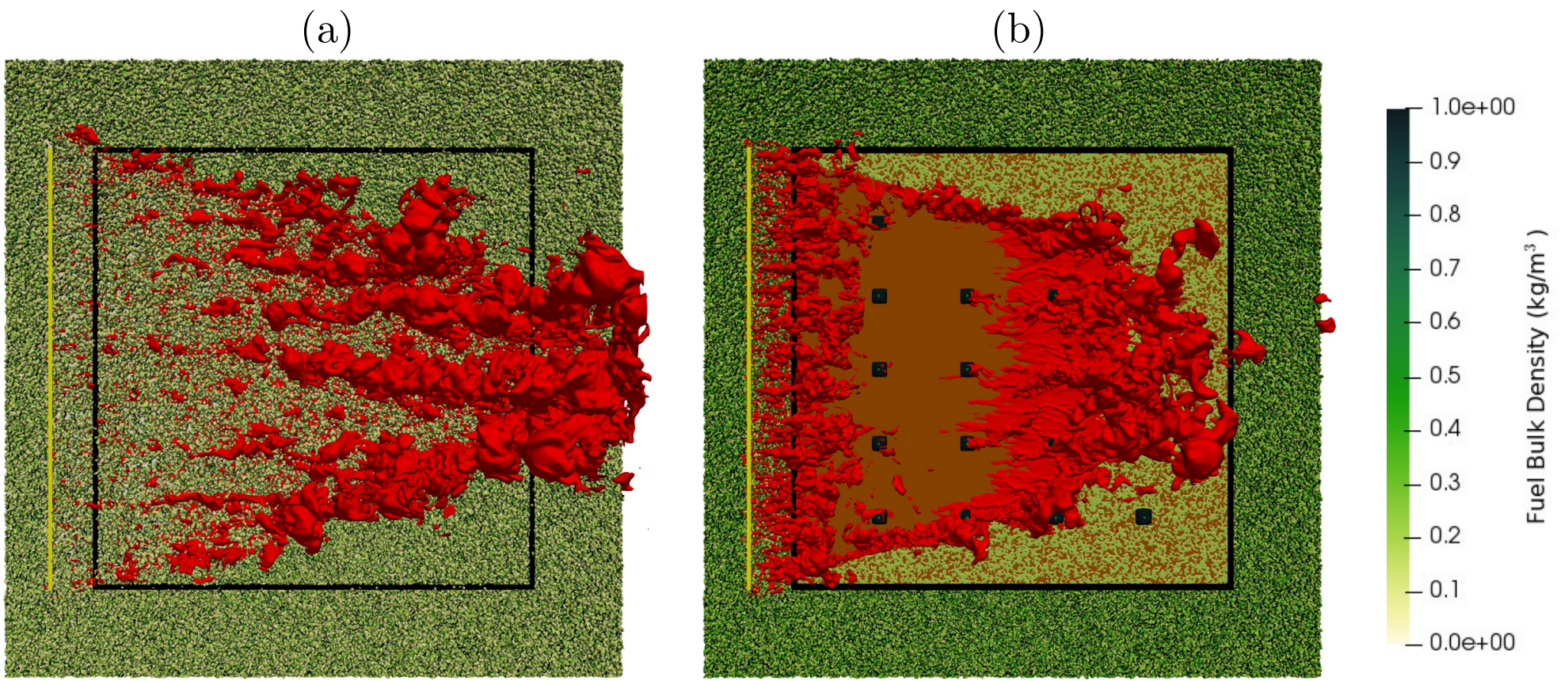
(a)
(b)
1.0e+00
0.9
0.8
0.7
0.6
0.5
0.4
0.3
0.2
0.1
0.0e+00
Fuel Bulk Density (kg/m^3)

Figure 3.

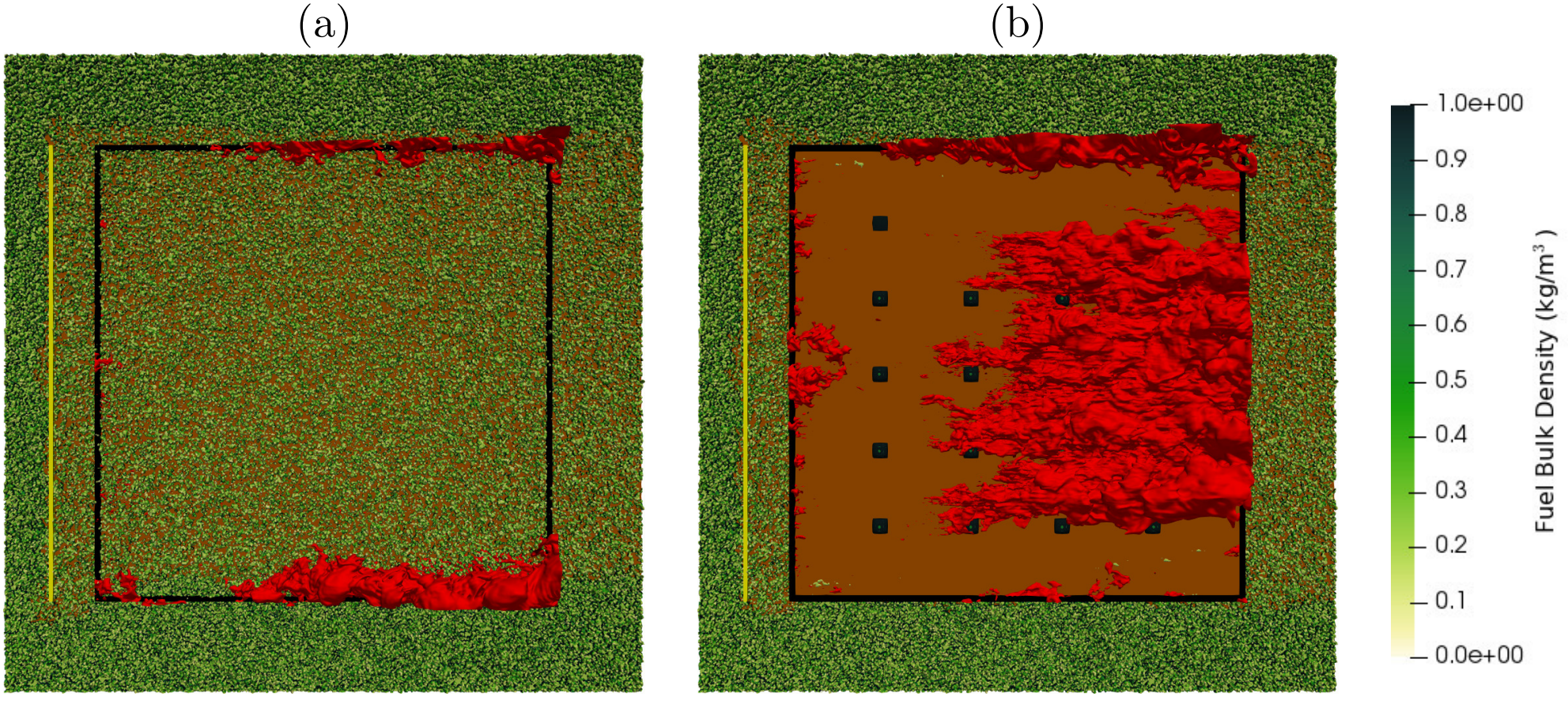
(a)
(b)
1.0e+00
0.9
0.8
0.7
0.6
0.5
0.4
0.3
0.2
0.1
0.0e+00
Fuel Bulk Density (kg/m^3)

Figure 4.

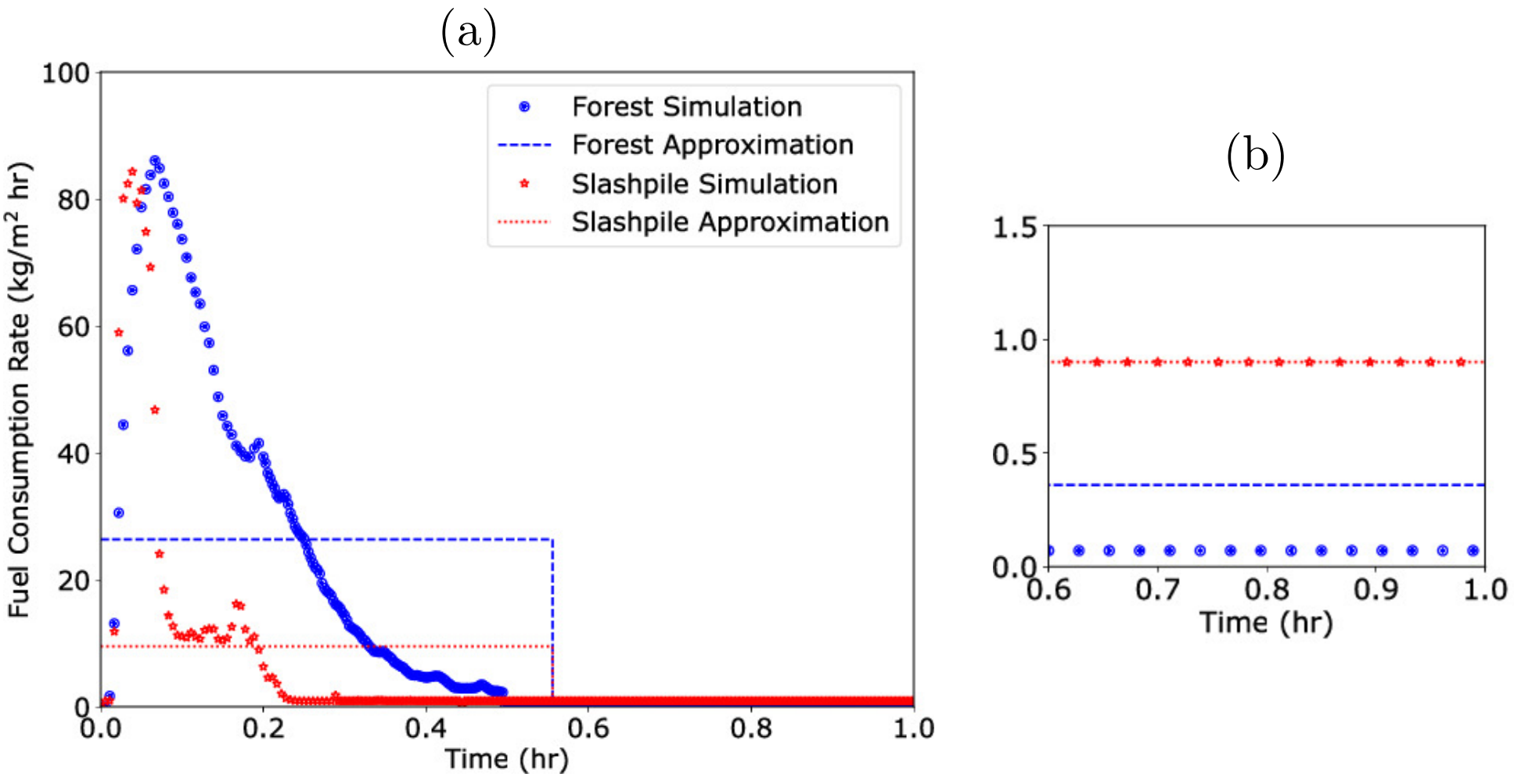
(a)
Forest Simulation
Forest Approximation
Slashpile Simulation
Slashpile Approximation
Fuel Consumption Rate (kg/m² hr)
Time (hr)
0
20
40
60
80
100
0.0
0.2
0.4
0.6
0.8
1.0
(b)
0.0
0.5
1.0
1.5
0.6
0.7
0.8
0.9
1.0
Time (hr)

Figure 5.

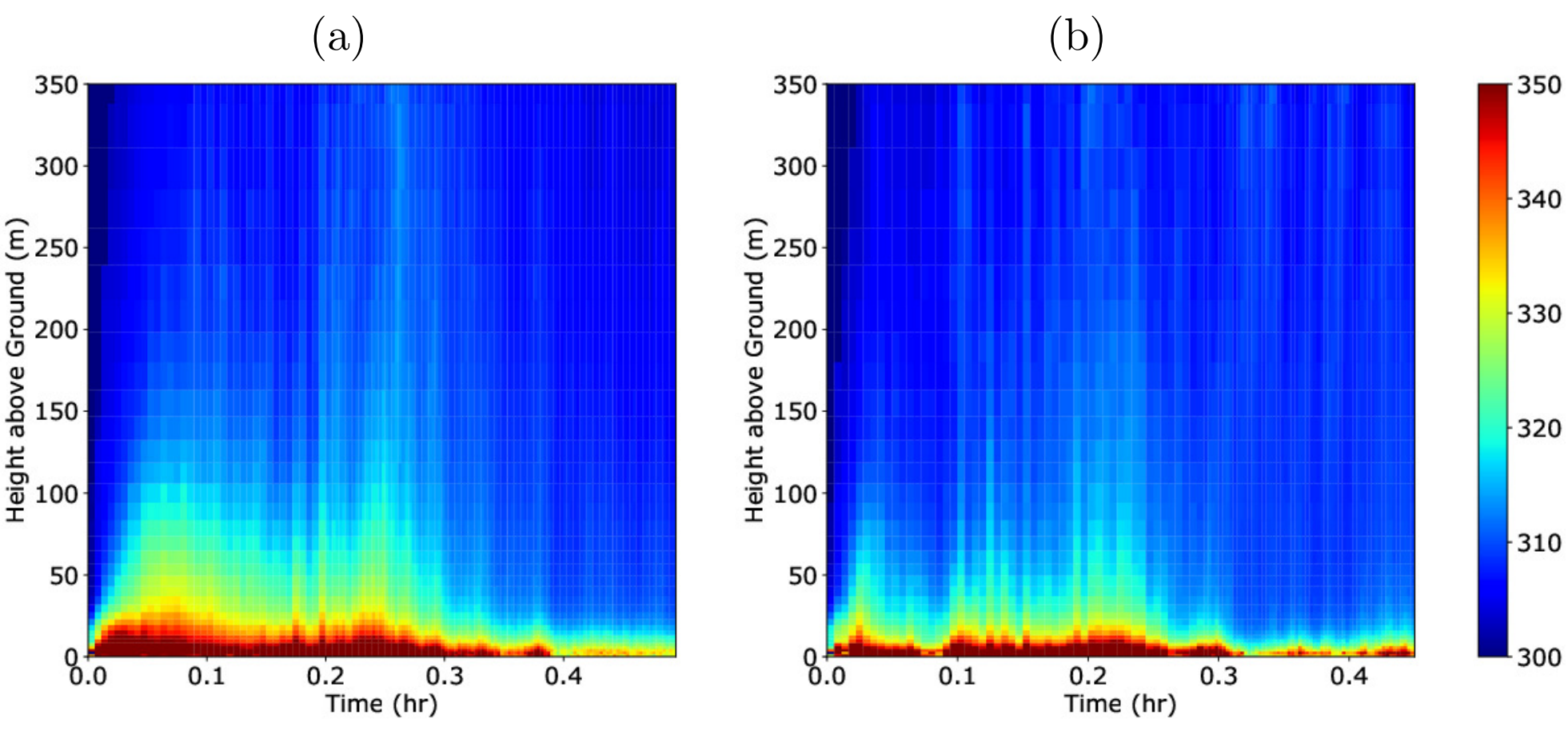
(a)
(b)
Height above Ground (m)
Time (hr)
0
50
100
150
200
250
300
350
0.0
0.1
0.2
0.3
0.4
300
310
320
330
340
350

Figure 6.

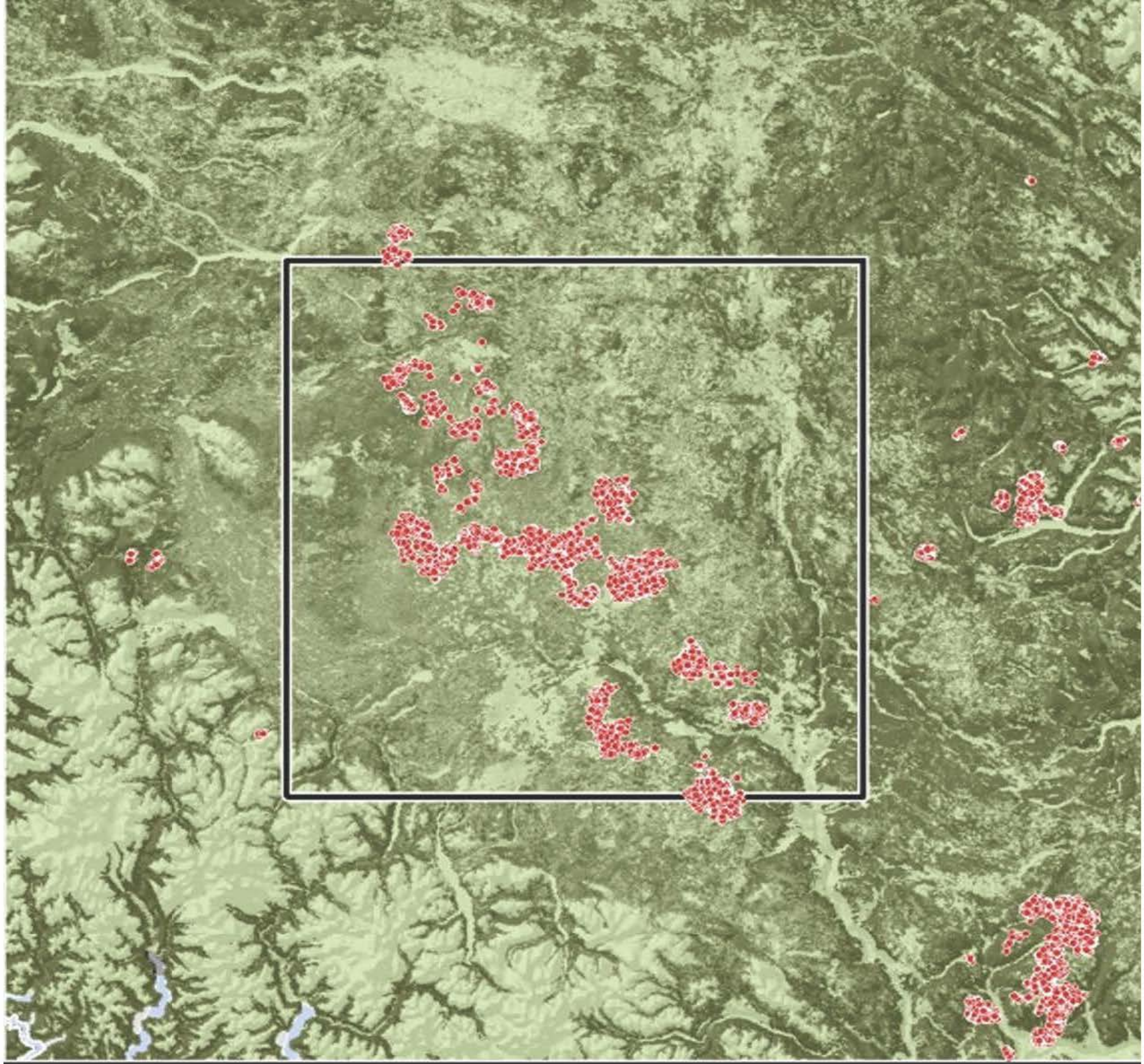

Figure 7.

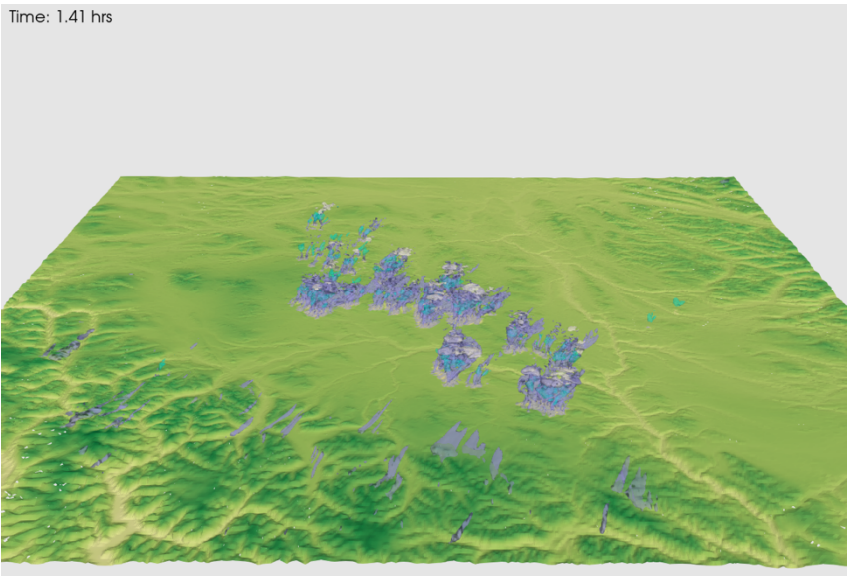
Time: 1.41 hrs

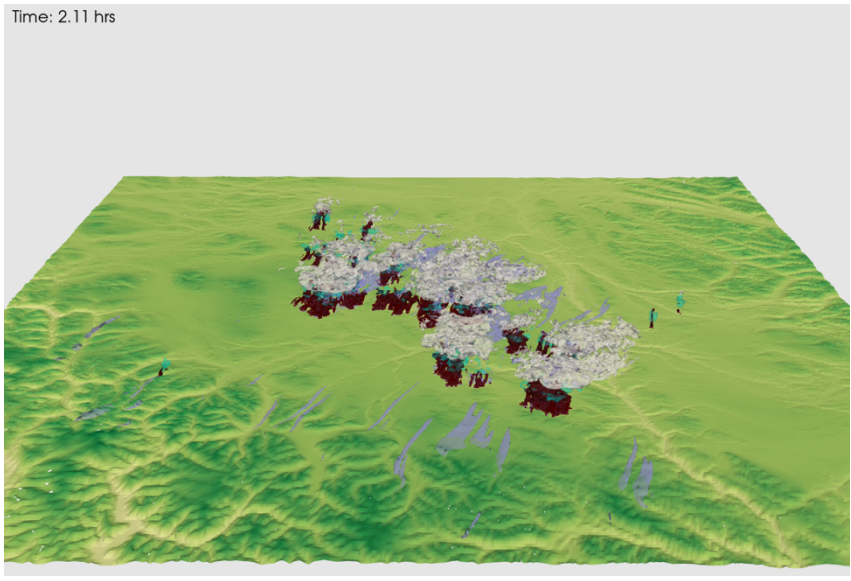
Time: 2.11 hrs

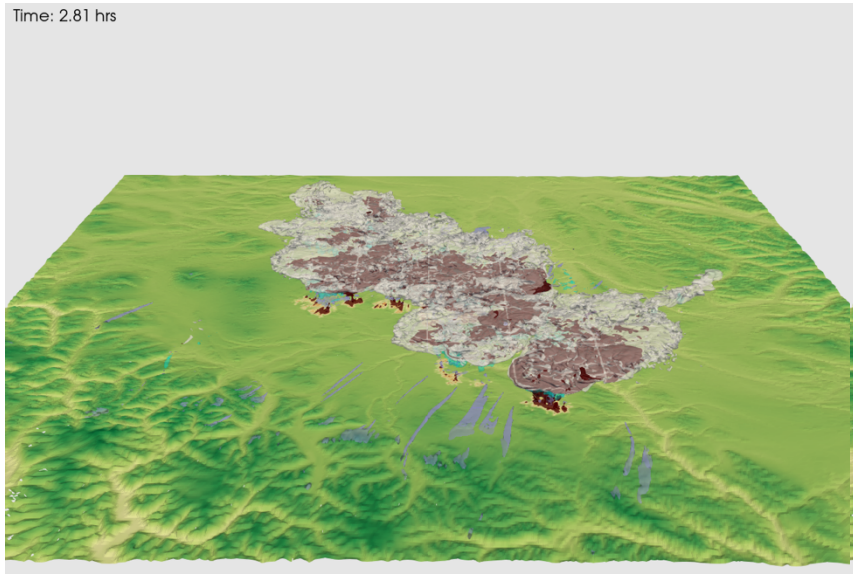
Time: 2.81 hrs

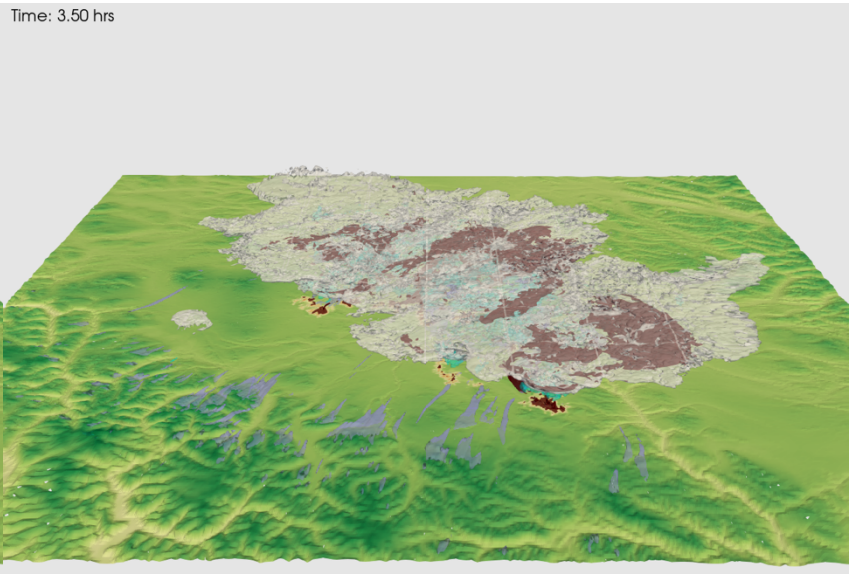
Time: 3.50 hrs

Figure 8.

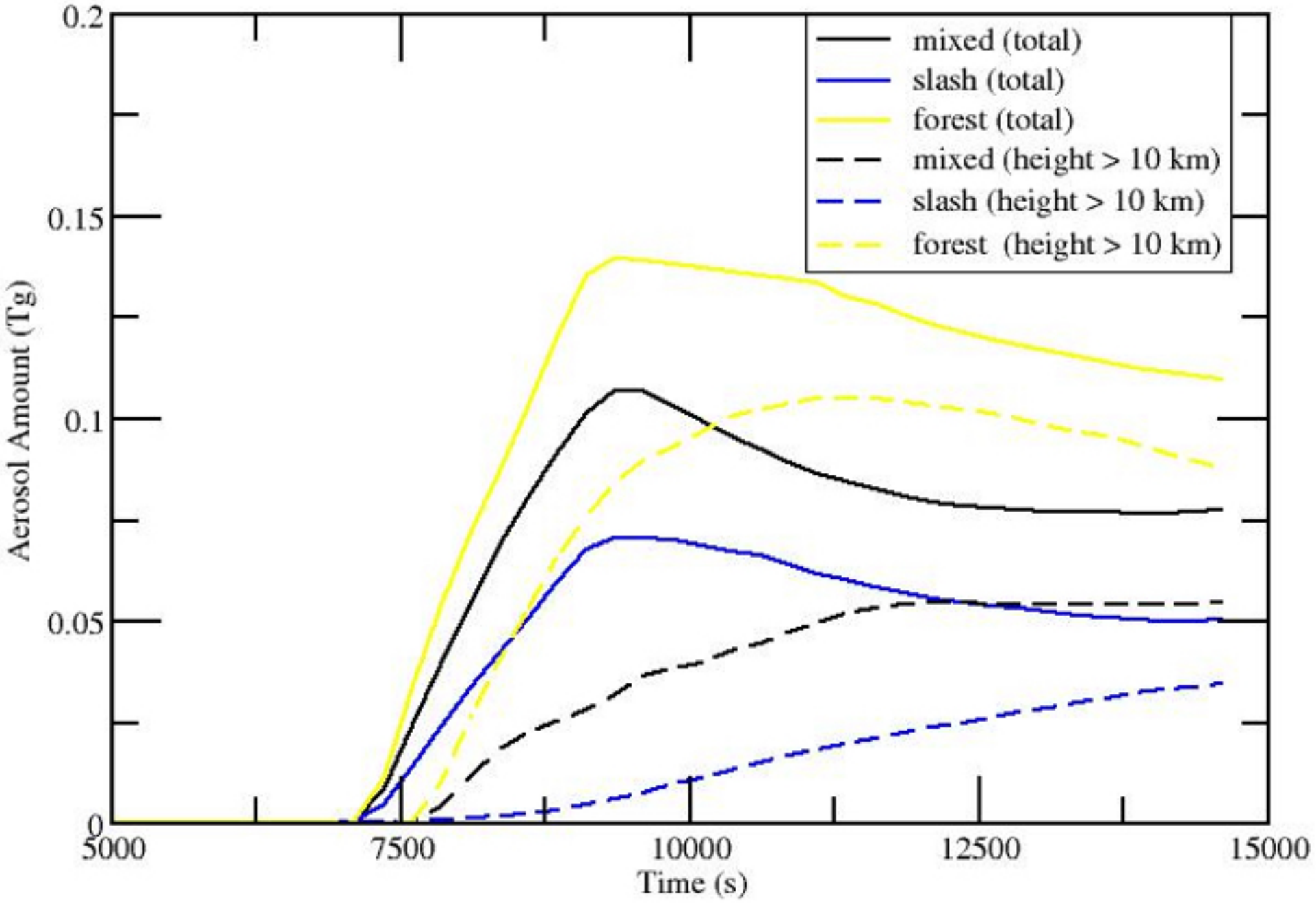
mixed (total)
slash (total)
forest (total)
mixed (height > 10 km)
slash (height > 10 km)
forest (height > 10 km)
Aerosol Amount (Tg)
0.2
0.15
0.1
0.05
0
5000
7500
10000
12500
15000
Time (s)

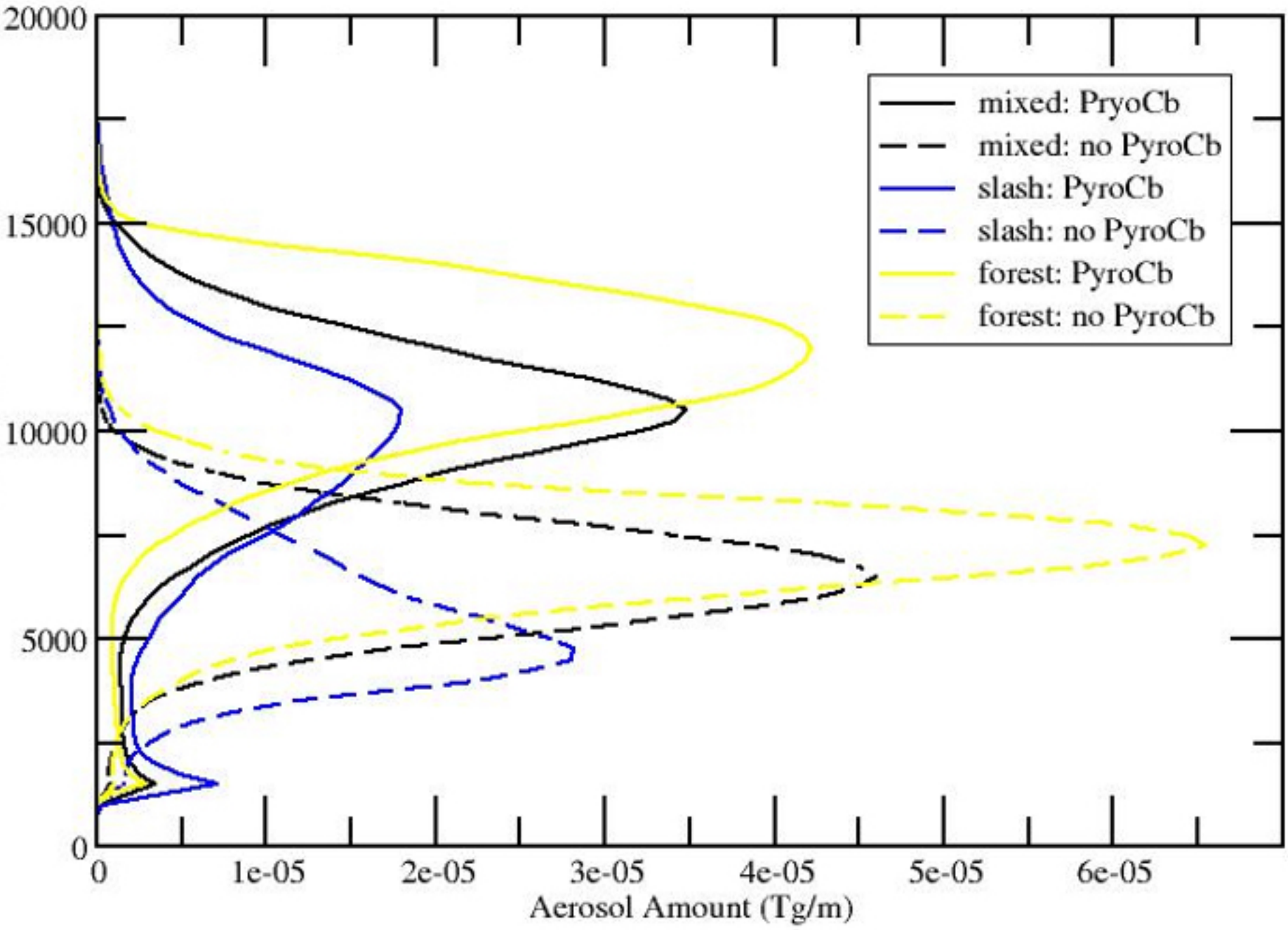
mixed: PryoCb
mixed: no PyroCb
slash: PyroCb
slash: no PyroCb
forest: PyroCb
forest: no PyroCb
Height (m)
20000
15000
10000
5000
0
0
1e-05
2e-05
3e-05
4e-05
5e-05
6e-05
Aerosol Amount (Tg/m)

Figure 9.

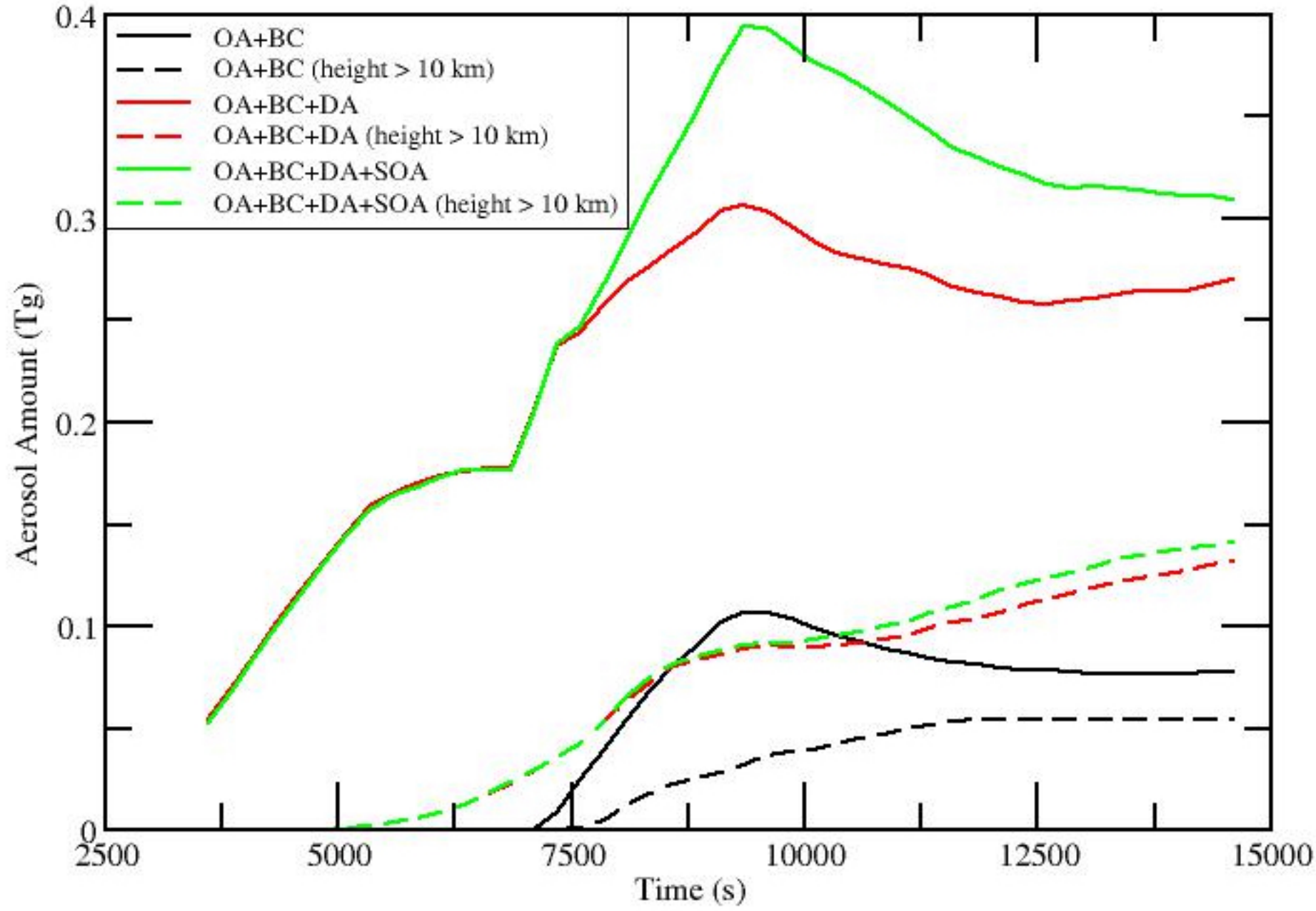
OA+BC
OA+BC (height > 10 km)
OA+BC+DA
OA+BC+DA (height > 10 km)
OA+BC+DA+SOA
OA+BC+DA+SOA (height > 10 km)
Aerosol Amount (Tg)
0.4
0.3
0.2
0.1
0
2500
5000
7500
10000
12500
15000
Time (s)

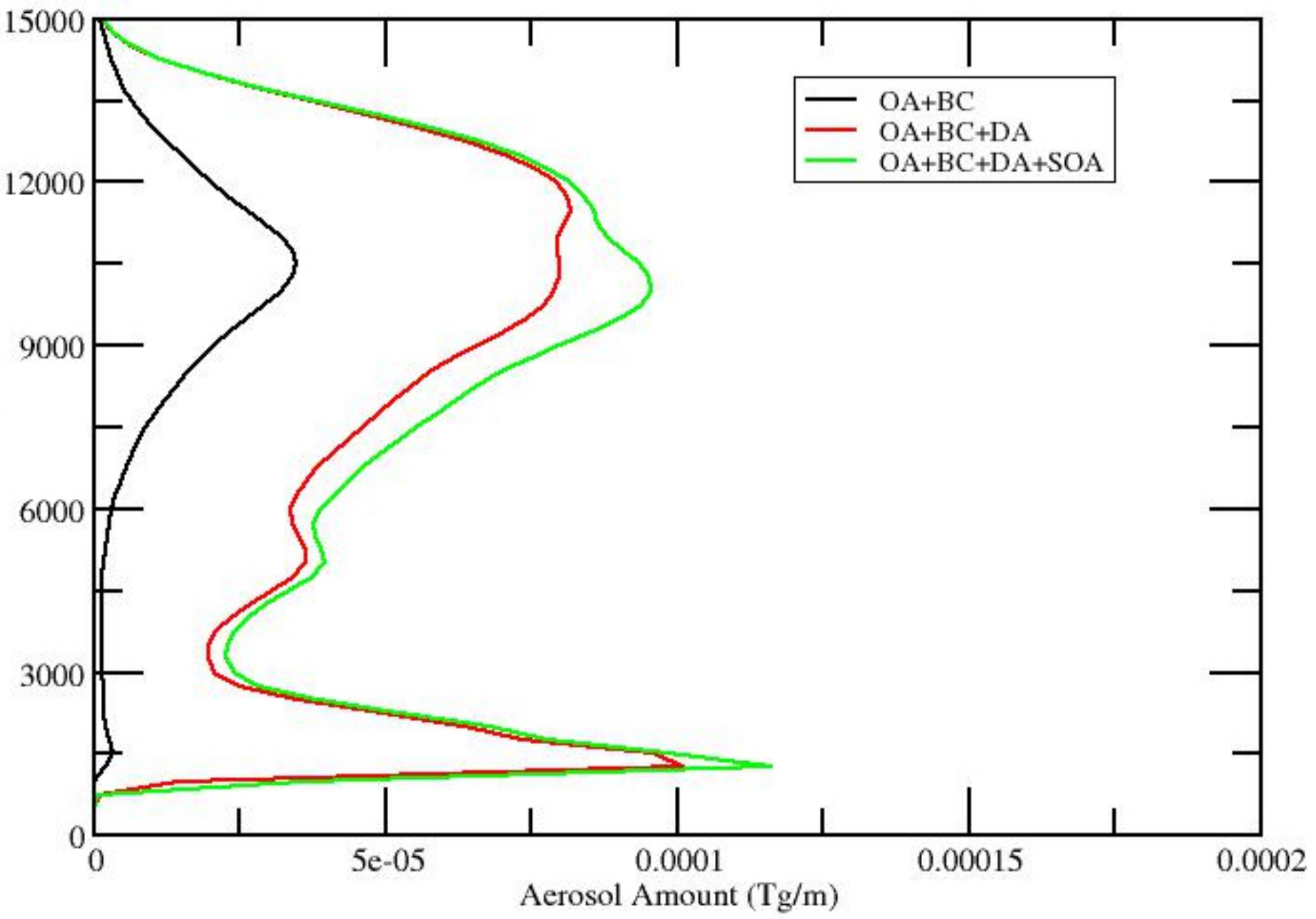
OA+BC
OA+BC+DA
OA+BC+DA+SOA
Height (m)
15000
12000
9000
6000
3000
0
0
5e-05
0.0001
0.00015
0.0002
Aerosol Amount (Tg/m)

Figure 10.

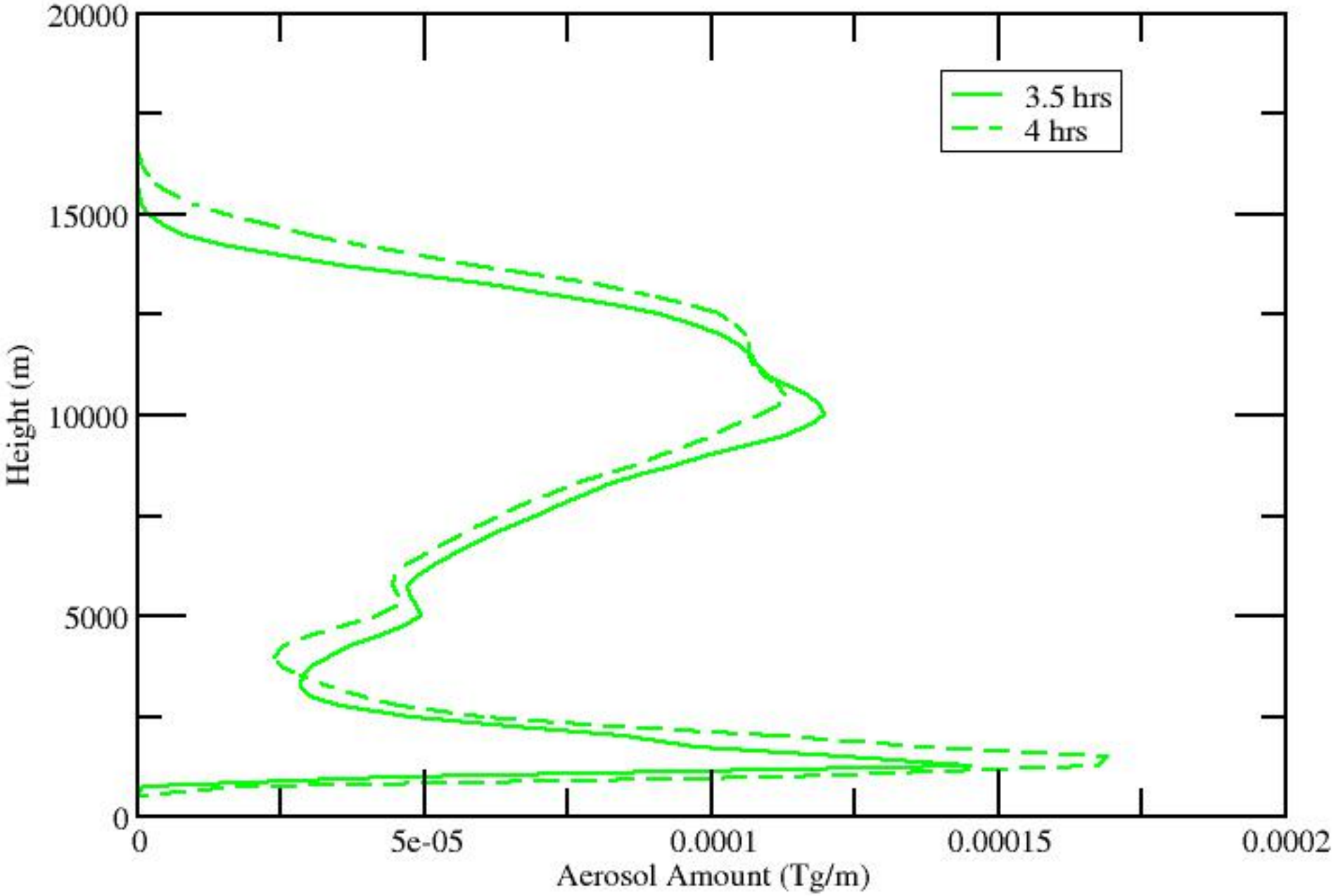
20000
15000
10000
5000
0
Height (m)
0
5e-05
0.0001
0.00015
0.0002
Aerosol Amount (Tg/m)
3.5 hrs
4 hrs

Figure 11.

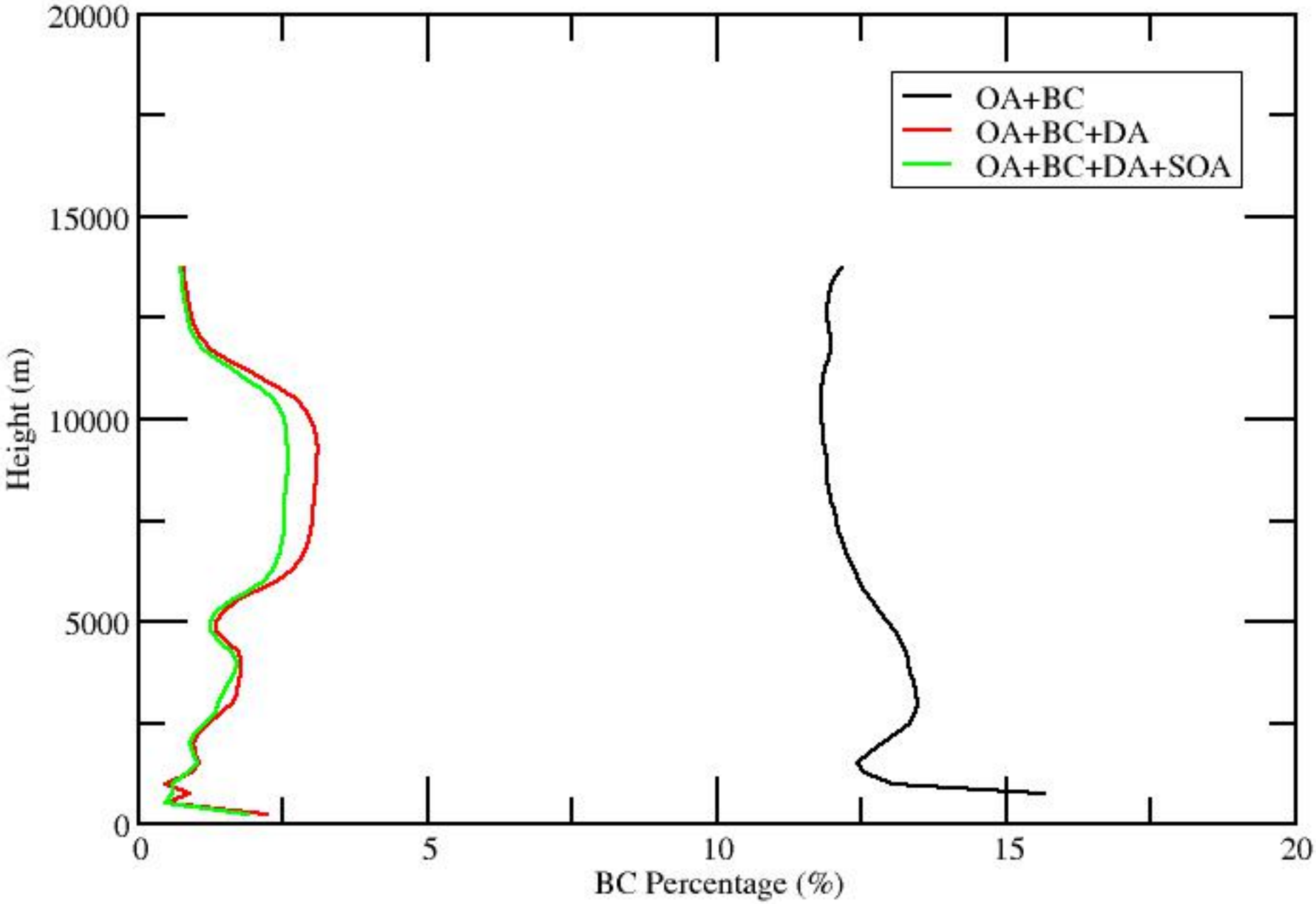
20000
15000
10000
5000
0
Height (m)
0
5
10
15
20
BC Percentage (%)
OA+BC
OA+BC+DA
OA+BC+DA+SOA